UNIVERSITÉ DU QUÉBEC À MONTRÉAL

SENSIBILITÉ DE LA PRÉCIPITATION À LA RÉSOLUTION HORIZONTALE DANS LE MODÈLE RÉGIONAL CANADIEN DU CLIMAT

MÉMOIRE
PRÉSENTÉ
COMME EXIGENCE PARTIELLE
DE LA MAÎTRISE EN SCIENCES DE L'ATMOSPHÈRE

PAR
MICHAEL JR. POWERS

SEPTEMBRE 2011

REMERCIEMENTS

J'aimerais d'abord remercier mon directeur de recherche, Dr. Daniel Caya pour son support scientifique, sa patience et pour sa disponibilité à travers ce périple de plusieurs mois. Je voudrais également remercier mon co-directeur, Dr. René Laprise pour son support. De plus, j'aimerais souligner et remercier le Centre pour l'Étude et la Simulation du Climat à l'Échelle Régionale (Centre ESCER) de l'UQÀM, pour son appui financier durant mes études de cycle supérieur. Je tiens également à remercier tous les membres de l'équipe de Simulations Climatiques à Ouranos pour leur aide et leurs réponses en lien avec le Modèle Régional Canadien du Climat (MRCC). Je me dois aussi de souligner le support informatique constant de Mourad Labassi à Ouranos. Finalement, je remercie ma mère, mon père, ainsi que ma copine pour leur soutien moral et leurs encouragements constants tout au long de ce cheminement.

TABLE DES MATIÈRES

LISTE DES FIGURES

LISTE DES TABLEAUX

LISTE DES ABRÉVIATIONS, SIGLES ET ACRONYMES

APA	Annual Precipitation Amount
BKF	Bechtold-Kain-Fritsch
CLASS	Canadian LAnd Surface Scheme
CGCM	Coupled Global Circulation Model
CRCM	Canadian Regional Climate Model
CRCM4	Canadian Regional Climate Model (4^{th} version)
CRCMD	Canadian Regional Modelling and Diagnostics
DAI	Data Access and Integration
DPE	Daily Precipitation Event
ESCER	Étude et la Simulation du Climat à l'Échelle Régionale
EAST CAN	Eastern Canada
GCM	Global Circulation Model
HPE	Hourly Precipitation Event
IPCC	Intergovernmental Panel of Climate Change
ISBA	Interactions Soil-Biosphere-Atmosphere
LAM	Limited-Area Model
MCG	Modèle de Circulation Générale
MCGC	Modèle de Circulation Générale Couplé
MRC	Modèle Régional du Climat
MRCC	Modèle Régional Canadien du Climat
MRCC4	Modèle Régional Canadien du Climat (4^{e} version)
NCEP	National Centers for Environmental Prediction
PCIC	Pacific Climate Impacts Consortium
PE	Precipitation Event
PF	Precipitation Frequency
PI	Precipitation Intensity
RCM	Regional Climate Model
UQÀM	Université du Québec à Montréal
WEST CAN	Western Canada

RÉSUMÉ

À l'aide de la quatrième génération du Modèle Régional Canadien du Climat (MRCC4), deux paires de simulations pilotées à leurs frontières par les réanalyses NCEP NRA-2 ont été créées pour deux régions distinctes du Canada : 1) l'ouest canadien (WEST CAN), et 2) l'est canadien (EAST CAN). Pour ces deux régions, chaque paire de simulations consiste en une simulation dont la résolution horizontale est de 15 km (vrai à 60° N) et une simulation dont la résolution horizontale est de 45 km (vrai à 60° N). En utilisant ces simulations, cette étude tente de déterminer l'impact de l'augmentation de la résolution horizontale sur le champ de précipitation du modèle. Les résultats montrent que l'augmentation de la résolution horizontale permet d'obtenir une représentation plus réaliste de la topographie dans les simulations à 15 km, puisqu'elles illustrent de plus fines caractéristiques du terrain, tels que d'étroites et profondes vallées ainsi que de hauts, mais petits, complexes montagneux. De plus, notre étude révèle que les simulations à 15 km produisent davantage de convergence d'humidité et d'évapotranspiration, menant ainsi à une augmentation de la précipitation. L'augmentation de la résolution permet à la simulation à 15 km de produire de la neige durant toute l'année au sommet des plus hautes montagnes du domaine WEST CAN. Pour le domaine EAST CAN, la précipitation totale et solide plus grande retrouvée dans la simulation à 15 km mène à un ruissellement supérieur à celui retrouvé dans la simulation à 45 km.

En comparant la précipitation simulée avec la précipitation observée provenant du réseau de stations d'Environnement Canada mesurant la précipitation horaire, on trouve que les simulations à 15 km produisent une distribution de la fréquence des précipitations horaires et une distribution de l'intensité des précipitations plus réaliste. Contrairement aux simulations à 15 km, les simulations à 45 km produisent moins d'événements horaires d'intensité modérée à très forte (3-10 mm/h) que ce qui est observé. Néanmoins, autant les simulations à 15 km que celles à 45 km produisent un biais positif en termes de fréquence et d'intensité des événements horaires de faibles intensités (0,2-3 mm/h). Conséquemment, une trop grande quantité de précipitation est générée annuellement par ce type d'événements, comparativement aux observations. La précipitation simulée est alors généralement plus grande que celle observée. Notre étude révèle également que pour analyser la fréquence et l'intensité de la précipitation, il est plus approprié d'utiliser une période d'accumulation d'une heure plutôt qu'une période d'accumulation de 24 heures. En effet, cela nous permet de comprendre plus facilement quels types d'événements le modèle est capable de reproduire et quelle est la contribution (en termes de quantité de précipitation) de chacun de ces événements.

Mots clés : modélisation régionale du climat, haute résolution, précipitation, MRCC

INTRODUCTION

L'eau est une ressource primordiale sur Terre, puisque c'est grâce à sa présence que la vie est possible. De plus, la coexistence simultanée des trois phases de l'eau (vapeur, liquide et solide) fait la particularité de notre planète (Webster, 1994). Sous une de ces trois phases, d'importantes quantités d'eau sont échangées entre les océans, l'atmosphère, le continent (l'eau des sols et l'eau de surface), la cryosphère et la biosphère. Ceci forme le cycle hydrologique. Ce cycle contrôle le climat à travers plusieurs interactions complexes (Peixoto and Oort, 1992). Sous l'action du rayonnement solaire, l'eau provenant des océans et des surfaces continentales est introduite dans l'atmosphère par évapotranspiration. Elle est transportée par le vent en phase vapeur, pour ensuite être condensée et stockée dans les nuages. Elle retombe finalement à la surface sous forme de précipitation liquide ou solide. Ceci constitue la branche atmosphérique du cycle hydrologique. Une fois précipitée à la surface, l'eau peut s'infiltrer dans le sol ou ruisseler (surface ou souterrain), ce qui alimente les cours d'eau et les océans. L'eau demeurée en surface ou absorbée par les plantes est ensuite évapotranspirée à nouveau et le cycle se poursuit. Ceci constitue la branche terrestre du cycle hydrologique. Parmi toutes les composantes du cycle hydrologique, la précipitation est probablement celle qui influence les plus nos activités quotidiennes (loisirs, travail, etc.). Il est donc primordial de connaître de quelle façon cette variable météorologique évoluera avec les changements climatiques. Afin de simuler le climat futur, les scientifiques ont maintenant recours à des modèles climatiques.

Depuis quelques années, plusieurs études ont été menées dans le but d'évaluer la capacité des modèles climatiques à simuler la précipitation (Mearns et al., 1995; Chen et al., 1996; Giorgi et Marinucci, 1996; Dai et al., 1999; Gutowski Jr. et al., 2003; Sun et al. 2006). Ces études ont montré que la plupart des modèles sont capables de reproduire la distribution spatiale de la précipitation, mais qu'ils ont de la difficulté à bien reproduire d'autres caractéristiques importantes de cette variable, tel que le cycle diurne, la fréquence et l'intensité. En utilisant la précipitation simulée par 18 Modèles de Circulation Généraux Couplés (MCGC), Sun et al. (2006) ont déterminé que la plupart des modèles surestiment la

fréquence de la précipitation faible (1-10 mm/jour) tout en reproduisant adéquatement l'intensité de ce type d'événements. Pour les événements de précipitation forte (> 10 mm/jour) toutefois, la pluparts des MCGCs sont capable de reproduire adéquatement la fréquence observée, mais ils en sous-estiment l'intensité. Une autre étude, réalisée par Christensen et al. (1998), a permis de démontrer que les Modèles Régionaux du Climat (MRCs) possèdent des difficultés semblables. En effet, les auteurs établissent que les MRCs surestiment généralement la fréquence des événements de trace de précipitation (< 0.1 mm/jour) et qu'ils sous-estiment la fréquence de la précipitation faible à forte (> 0.1 mm/jour). De plus, d'autres études antérieures ont permis de découvrir que les modèles climatiques produisent typiquement davantage d'événements de faibles intensités par rapport à ce qui est observé (Mearns et al., 1995; Chen et al., 1996; Giorgi et Marinucci, 1996; Dai et al., 1999; Gutowski Jr. et al., 2003). Les modèles climatiques actuels doivent mieux reproduire la fréquence et l'intensité de la précipitation pour ainsi pouvoir prévoir adéquatement leur changement en climat futur. Par ailleurs, l'augmentation des gaz à effet de serre semble entrainer une augmentation de la fréquence des événements de précipitation forte, de même qu'un accroissement de la fréquence des sécheresses. Résultant d'une augmentation de la température et de l'humidité spécifique, une amplification du cycle hydrologique est ainsi prévue (Trenberth, 1999; Trenberth, 2003). Donc, étant donné que ces changements auront un impact important sur l'activité humaine, il est primordial que les modèles soient très habiles à simuler ces caractéristiques de la précipitation.

De nos jours, l'utilisation d'un MRC à aire limitée au-dessus d'une région d'intérêt est le principal moyen de simuler les caractéristiques régionales de la précipitation. Les MRCs permettent une représentation plus fine de l'échelle spatiale que les Modèles de Circulation Généraux (MCGs). Présentement, la plupart des modèles à aire limitée opérationnels ont une résolution horizontale variant entre 20 et 50 km. Même à ces résolutions, la topographie n'est pas parfaitement représentée et certains aspects du terrain sont tout de même manquants, ce qui peut avoir un impact significatif sur la simulation des différentes variables atmosphériques, principalement la précipitation. Bref, même à de telles résolutions horizontales, les processus de fines échelles (dont la résolution spatiale est supérieure à la résolution du MRC) ont besoin d'être paramétrés. Toutefois, les schémas de paramétrisation

sont une source d'incertitudes dans les simulations climatiques puisqu'ils sont basés sur des approximations et simplifications. D'ailleurs, un effort international est mené dans le but d'améliorer les schémas existant ou bien encore pour en créer de nouveaux afin que les processus de fines échelles soient mieux représentés dans les modèles numériques. Avec une augmentation de la résolution horizontale, la représentation des caractéristiques de surface devrait être meilleure, ce qui fait que les modèles devraient mieux résoudre les phénomènes de fines échelles. Certaines études ont été menées dans le passé pour connaître l'impact d'une augmentation de la résolution horizontale sur les champs atmosphériques. Dans leur étude, Christensen et al. (1998) ont analysé le comportement des composantes du cycle hydrologique simulées par un MRC et un MCG. Pour réaliser cette étude, les auteurs ont utilisé une technique de double-pilotage dans laquelle un MRC ayant une résolution horizontale de 19 km était piloté aux frontières par un autre MRC ayant une résolution horizontale de 57 km. Ce dernier MRC était lui piloté aux frontières par un MCGC. L'étude montre qu'en terrain montagneux, la simulation à haute résolution montrait d'importantes améliorations dans la représentation du ruissellement de surface et du couvert de neige. L'étude montre également que la distribution de la précipitation selon différentes classes d'intensités est plus réaliste avec la simulation à haute résolution.

L'objectif de la présente étude est d'évaluer l'impact de l'augmentation de la résolution horizontale sur la précipitation, aussi bien que sur d'autres composantes du cycle hydrologique, simulés avec la quatrième génération du Modèle Régional Canadien du Climat (MRCC4) au-dessus de deux régions climatiques distinctes. Les simulations du MRCC4 sont en fait produites au-dessus de deux domaines de l'Amérique du Nord : 1) centré sur la province de la Colombie-Britannique (ouest canadien) et 2) centré sur la province du Québec (est canadien). Pour chacune de ces régions, une paire de simulations d'une durée de quatre ans, pilotée aux frontières par les réanalyses NCEP NRA-2 est analysée. Cette paire de simulations consiste en une simulation ayant une résolution horizontale de 15 km, et une simulation ayant une résolution horizontale de 45 km.

Ce mémoire est écrit sous la forme d'un article. La première partie comprend un court résumé des études antérieures portant sur la précipitation simulée par les modèles climatiques

(MRCs et MCGs), un bref descriptif du MRCC et une description de la méthodologie utilisée. La convergence d'humidité, l'évapotranspiration, la précipitation (totale, liquide et solide), la température à 2 m, l'équivalent en eau de la neige, le ruissellement de surface et le nombre de jours de précipitation par année constituent les champs météorologiques simulés qui seront étudiés de plus près. La précipitation simulée par le MRCC est également comparée avec la précipitation horaire observée, tout en portant une attention particulière à la fréquence et l'intensité de la précipitation.

CHAPITRE I

Sensitivity of precipitation to horizontal resolution within the Canadian Regional Climate Model

Michael Jr. Powers [1,3], Daniel Caya [1,2,3] and René Laprise [1,3]

[1] *Canadian Regional Modelling and Diagnostics (CRCMD) Network, Université du Québec à Montréal*

[2] *Ouranos Consortium Climate Simulations Team*

[3] *Centre pour l'étude et la simulation du climat à l'échelle régionale (ESCER Center)*

Septembre 2011

Corresponding author address:

Michael Jr. Powers

Dép. Sciences de la terre et de l'atmosphère

Université du Québec à Montréal (UQÀM)

201, President-Kennedy Avenue, 6th floor

Montréal, QC, Canada, H2X 3Y7

E-mail: powers@sca.uqam.ca

Abstract

Using the fourth generation of the Canadian Regional Climate Model (CRCM4), two pairs of 4-year simulations forced at their boundaries by the NCEP NRA-2 reanalyses are performed over two different regions of Canada: 1) western Canada (hereafter WEST CAN) and 2) eastern Canada (hereafter EAST CAN). For both regions, each pair of simulations consists of one 15-km resolution (true at 60°N) run and one 45-km resolution (true at 60 °N) run. Using these simulations, this study investigates the impact of increasing horizontal resolution on the precipitation field. Results show that increasing horizontal resolution allows a more realistic representation of the topography in the 15-km simulations, by showing smaller scale features such as long and narrow valleys as well as high and narrow mountains. This investigation also reveals that the 15-km simulations produce more water vapour convergence and more evapotranspiration, which leads to an increase of precipitation in the 15-km simulations. The higher resolution also allows the 15-km simulation to capture some of the permanent snow present at the top of the high mountains within the WEST CAN domain. Over the EAST CAN domain, the greater 15-km total and solid precipitation leads to more runoff than within the 45-km simulation.

When comparing simulated precipitation with observed precipitation from Environment Canada's hourly precipitation network, it is found that the 15-km simulations depict more realistic hourly precipitation frequency (hereafter PF) and precipitation intensity (hereafter PI) distributions than the 45-km simulations. Contrary to the 15-km simulations, the 45-km simulations produce less moderate-to-very-heavy (3-10 mm/h) hourly precipitation events (hereafter HPE) than those observed. Nevertheless, both simulations produce a positive bias in the frequency and intensity of light HPE (0.2-3 mm/h), which leads to an annual precipitation amount too large, in comparison with observations, generated by those events. Thus, the simulated precipitation tends to be greater than the observed precipitation. Our investigation also revealed that using an hourly accumulation interval to analyse the PF and PI was more appropriate than using a daily accumulation interval in understanding which events the model is able to reproduce and what the contribution (in precipitation amount) of each type of event is.

1 Introduction

Over the recent years, many studies have been carried out to see how well climate models simulate precipitation (Chen et al. 1996, Dai et al. 1999, Gutowski Jr. et al. 2003, Sun et al. 2006). These studies showed that most models can usually reproduce the spatial distribution and climatological mean of precipitation, but tend to fail in reproducing some other important features of this atmospheric variable, such as the diurnal cycle, the frequency and the intensity. Using 18 different Coupled Global Circulation Models (CGCMs), Sun et al. (2006) found out that most models overestimate the frequency of light precipitation (1-10 mm/day) but reproduce adequately the intensity of those events. For heavy precipitation (> 10 mm/day), their study revealed that most CGCMs are able to reproduce quite properly the observed frequency, but underestimate the intensity of such events. Another study realised by Christensen et al. (1998) showed that Regional Climate Models (RCMs) have similar difficulties. Indeed, the authors found that RCMs tend to underestimate the frequency of trace precipitation events (< 0.1 mm/day) while they overestimate the frequency of low-to-heavy precipitation events (> 0.1 mm/day). Moreover, other past studies discovered that climate models produce typically more light precipitation events than what is observed (Mearns et al. 1995, Chen et al. 1996, Giorgi et Marinucci 1996, Dai et al. 1999, Gutowski Jr. et al. 2003). Thus, the frequency and intensity of precipitation need to be well reproduced by climate models to adequately project their change in future climate. Besides, the frequency of heavy precipitation events is expected to increase, as well as the frequency of droughts. An enhancement of the hydrological cycle is also expected resulting from the increase in air temperature and specific humidity (Trenberth 1999, Trenberth 2003). Since these changes will have significant impacts on human activities, there is a real need for models to have very good skills in simulating these precipitation features.

Nowadays, the use of a limited-area (LAM) RCM over an area of interest is the principal way to simulate regional characteristics of precipitation. RCMs allow a finer representation of the spatial scale than a GCM. Currently, most operational LAMs have a horizontal resolution of about 20 to 50 km. Even at these resolutions, the surface topography is not

perfectly represented and some aspects of the terrain are still missed, which can have significant impacts in simulating properly the different atmospheric variables, especially precipitation. Therefore, even at these horizontal resolutions, small-scale processes (whose spatial scales are smaller than the RCM resolution) still need to be parameterized. The parameterization schemes are sources of uncertainties in simulations since they are based on many approximations and assumptions. As a result, an important work is made internationally to improve the existing schemes or to create new ones to better represent the small-scale processes within models. With an increase in horizontal resolution, the model should better resolve more small-scale features resulting from an improved representation of the land surface characteristics. Studies have been carried out in the past to investigate the influence of increased horizontal resolution on the simulated atmospheric fields. Christensen et al. (1998) analyzed the behavior of the components of the hydrological cycle as simulated by an RCM and a GCM. In a double-nesting approach over Scandinavia, the authors used a 19-km horizontal resolution RCM nested into a 57-km horizontal resolution RCM simulation, which in turn was driven by a Coupled GCM (CGCM). They found that in mountainous regions, the high-resolution simulation showed improvements in the representation of runoff and snow cover. They also found that the distribution of precipitation on different intensity classes was more realistic when simulated by the high-resolution simulation.

The objective of this study is to investigate the impact of increasing horizontal resolution on precipitation as well as on other components of the hydrological cycle within the fourth generation of the Canadian Regional Climate Model (CRCM4) over two very distinct climate regions. CRCM4 simulations are performed over two different domains of North America: 1) centered over the province of British-Colombia (Western Canada), and 2) centered over the province of Québec (Eastern Canada). For each region, a pair of 4-year simulations forced at their boundary by the reanalysis NCEP NRA-2 is analyzed. This pair of simulations consists in one 15-km horizontal resolution run to be compared to a one 45-km horizontal resolution run. Precipitation, screen temperature and other components of the hydrological cycle (convergence of humidity, evapotranspiration, liquid and solid precipitation, runoff, snow water equivalent and number of wet days) produced by those simulations are analyzed. The

model precipitation outputs are then compared to hourly-precipitation observations. Throughout this study, an emphasis is put on the frequency and intensity of precipitation.

The text is organised as follow: section 2 gives a brief description of the model used. Section 3 presents the experiments and methodology, with a description of the model simulations and observations employed, as well as the model-observation comparison methodology. Section 4 presents the results obtained through this study. Finally, section 5 gives a summary and concludes.

2 Model Description

Originally developed at the *Université du Québec à Montréal* (UQAM), the CRCM is a limited-area model (LAM) driven at its boundaries by the large-scale circulation from either reanalyses or global climate models. The model integrates the fully elastic nonhydrostatic Euler equations, which are solved by an off-centered semi-implicit and semi-Lagragian numerical algorithm (Caya 1996, Laprise et al. 1998, Caya and Laprise 1999). The CRCM horizontal grid is uniform in a polar stereographic projection and its vertical resolution is variable using the scaled terrain-following Gal-Chen coordinate. In the CRCM, the precipitation results from two processes: the large-scale precipitation (resolved) and the small-scale precipitation (parameterized). The large-scale precipitation arises from a simple supersaturation-based condensation scheme while the small-scale precipitation comes from the Bechtold-Kain-Fritsch (BKF) mass flux scheme (Bechtold et al. 2001; Paquin et al. 2002), adapted to the CRCM resolution. In this study, we use the fourth generation of the CRCM (CRCM4), which is the operational version of the model developed and used by the Ouranos Consortium Climate Simulations Team. This version of the model includes the version 2.7 of the Canadian LAnd Surface Scheme, CLASS2.7 (Verseghy 1991; Verseghy et al. 1993). The CRCM4 also allows spectral nudging, which is a method in which the model's large scales are partially or completely replaced by the nested long-waves at every time step (see Storch et al. 1999, Riette and Caya 2002, Alexandru et al. 2009). More informations on the CRCM4 can be found in Music and Caya (2008).

3 Experiments and methodology

3.1 Description of the model simulations

In this study, CRCM4 simulations are performed over two different regions of Canada: western Canada (hereafter WEST CAN) and eastern Canada (hereafter EAST CAN). These two domains (see Fig. 1 for geographical position of the domains) have been chosen for their different climate regime and physiography. The WEST CAN domain is a mountainous region (with summits reaching more than 4000 m) along the Pacific coast. The WEST CAN domain is almost always under the influence of a humid air flow coming from the Pacific Ocean toward the topographic barrier, which then represents an important factor in the formation of precipitation. In comparison to the WEST CAN domain, the EAST CAN domain has a much flatter terrain (with the highest mountain slightly above 1000 m) and the topography does not play as much an important role in the formation of precipitation as it does in western Canada. However, the domain is located in a Storm-Track corridor and many low-pressure systems from different origins cross the province of Québec. Those low pressure systems generally come from the Rocky Mountains, the Gulf of Mexico or the East Coast of United-States (Zishka and Smith, 1980).

For both regions (WEST CAN and EAST CAN), two 4-year-long (December 2001 to November 2005) simulations forced at their boundary by the NCEP NRA-2 reanalysis are used (Table 3.1). These two simulations consist in one 15-km-resolution (true at 60°N) run with a 5-minute time step and one 45-km-resolution (true at 60 °N) run with a 15-minute time step. Note that the simulations are originally performed from January 1999 to November 2005, from which a spin-up of 35 months has been taken off. Also, the spectral nudging was not applied in these runs because of the small size of the domains.

3.2 Description of the water cycle components analysis

The hydrological cycle controls and regulates climate in a fundamental way through many complex interactions (Peixoto and Oort, 1992). Therefore, our analysis in this study is not limited to the total precipitation, but also includes the main components of the hydrological cycle (convergence of humidity, evapotranspiration, liquid and solid precipitation and runoff) as simulated by the CRCM. Along with these components, we also analyse the surface temperature, snow water equivalent and number of wet days. For both domains, we qualitatively compare the 4-year annual mean of these 15-km CRCM-simulated variables to that of the 45-km CRCM-simulated variables. We also contrast the CRCM 15-km and 45-km domain averages of each variable, as well as their domain-averaged mean annual cycle.

As shown in Music and Caya (2007), the water cycle can be separated into two branches: atmospheric and terrestrial. Applying the law of water mass conservation in a given control volume leads to the water budget equation. The water budget equation for an atmospheric column (per unit area) can be written as

$$\frac{\partial W}{\partial t} = -\nabla_H \bullet \mathbf{Q} - P + E \tag{1}$$

where W (kg m^{-2}) is the precipitable water in the atmosphere, which represents the amount of water that would precipitate if all the water vapor in a column of the atmosphere were condensed, E (kg m^{-2} s^{-1}) is evapotranspiration, and P (kg m^{-2} s^{-1}) is precipitation. The operator ∇_H is the horizontal divergence and $\mathbf{Q}$ is the vertically integrated horizontal water vapor flux:

$$\mathbf{Q} = \int_{p_s}^{p_{top}} q\mathbf{V}\frac{dp}{g} \tag{2}$$

where q, $\mathbf{V}$, and g represent respectively the specific humidity, the horizontal velocity vector, and the gravitational acceleration. The lower limit in the integral (p_s) is the surface pressure and p_{top} is the pressure at the model lid.

In Equation 1, the term $-\nabla_H \bullet \mathbf{Q}$ is the horizontal convergence water vapor flux, C (hereafter convergence of humidity). Replacing the convergence of humidity term by C into Equation 1 leads to

$$\frac{\partial W}{\partial t} + P = C + E \tag{3}$$

Taking time and spatial averages of the atmospheric water budget equation (3) over a multiyear period and over the whole domain leads to

$$[\overline{P}] = [\overline{C}] + [\overline{E}] \tag{4}$$

where $\overline{X}$ is the time average of the component X, and $[X]$ is the domain average. The term $[\partial W / \partial t]$ can be neglected because it tends to zero when averaged over a long period of time (Music and Caya, 2007). When considering the 4-year annual mean domain average of these components, Equation 4 can be used. Precipitation occurs when the available water vapor condenses and falls on the ground. Thus, Equation 4 establishes that the water vapor available to generate precipitation can come from two different sources: convergence of humidity or evapotranspiration.

As fully explained in Music and Caya (2007), applying the water conservation law to a land column and then taking time and spatial averages of the terrestrial water budget equation over a multiyear period and over the whole domain leads to

$$[\overline{R}] = [\overline{P}] - [\overline{E}] \tag{5}$$

where R (kg m^{-2} s^{-1}) is the total runoff. Equation 5 can also be used when considering the 4-year annual mean domain average of these components. Equation 5 then establishes that the runoff is equal to the amount of water that precipitates minus the amount that goes back into the atmosphere through evapotranspiration.

3.3 Description of the observations

The observational data used in this study consist in the Environment Canada's hourly-precipitation network of weather stations (DAI Catalogue, 2009). Most of these stations are automatic and measure the hourly accumulation of precipitation with either a Fisher Porter or a tipping-bucket rain gauge. The threshold of these instruments may vary from one station to another with ranges between 0.1 mm/h and 0.2 mm/h. For this reason, we have chosen 0.2 mm/h has the common threshold for all the stations and then, any amount inferior to this is brought back 0 mm/h. For the present study, we only used the stations that are located into our two domains of interest, and we rejected the stations that had more than 50% of missing values through the 4-year period. This criterion left us with a total of 27 stations for the WEST CAN domain and of 45 stations for the EAST CAN domain (Fig. 2).

3.4 Model-observation comparison methodology

Over both domains, the simulated precipitation was compared to the observed precipitation following this procedure. First, we find the closest CRCM4 grid point (center of the grid-box at 15-km and 45-km) to each station, resulting in the same number of model grid points than of stations. The fact of choosing the closest CRCM grid point to a station has some consequences worth mentioning here: 1) the closest grid point may not necessarily be a land point in the model, and 2) some grid points may contain more than one station, meaning that one grid point may be the closest to two (or more) different stations. For the WEST CAN domain, the simulation W15 has 21 grid points out of 27 being considered as land while this number is 26 for the simulation W45. For the EAST CAN domain, the simulation E15 has 36 grid points out of 45 being considered as land while the simulation E45 has 32. In the 15-km simulations, the number of different grid points always equals the number of stations meaning that there is no more than one station falling in a grid point. However, in the 45-km simulations, some grid points contain two stations. In fact, the number of different grid points is 23 for the simulation W45 and 42 for the simulation E45.

Once the closest grid point to the station is found (for each domain), we then have three different hourly-precipitation time series (observed, CRCM4 15-km and CRCM4 45-km) that can be compared. While comparing these three time series, if there is a missing value in the observed time series, the corresponding simulated value is discarded. Then, we assign a value of 0 mm/h to any simulated precipitation values being below the instrument's threshold (0.2 mm/h). Next, using the hourly time series, we build the daily time series by accumulating precipitation over a 24-hour period. With these 4-year long time series, we calculate the following climatological 4-year means for each location: the annual cycle, the precipitation frequency per intensity interval, the precipitation intensity per intensity interval, and the cumulative annual precipitation amount per intensity interval. These variables have been chosen for the following reasons. First, as mentioned in the introduction, the frequency and intensity of precipitation is expected to change in future climate (Trenberth 1999, Trenberth 2003). Second, there is a need to find out if the model can correctly reproduce both the mean observed precipitation frequency and the mean observed precipitation intensity. Indeed, a model might simulate properly the mean precipitation rate over a region but this could come from a wrong combination of frequency and intensity. Plus, dividing precipitation in intensity intervals allows a better understanding of what kind of events the model has the best skill to reproduce.

4 Results and Discussions

4.1 WEST CAN domain

4.1.1 Analysis of precipitation

As mentioned in section *3.1*, topography plays a key role in the formation of precipitation over western Canada (WEST CAN domain). In winter, a flow of moist air is brought into the continent by a climatological surface pressure system known as the Aleutian low (located in middle north Pacific; Ahrens 2003). During summer, the Pacific high replaces the Aleutian low (Ahrens 2003), which reduces the transport of moist air into the region (especially in southern British Columbia, Canada) and then reduces precipitation. However, there is on average an almost constant southwesterly flow (at the surface) of humid air coming from the Pacific Ocean. Once brought over the continent, this moist air encounters a first topographic barrier along the Coastal Range. When reaching the barrier, this humid air is forced to rise, condense, and eventually to precipitate on the upwind side of the mountains, resulting in a strong band of precipitation maximum along the Pacific Coast as it can be seen in Figure 3. On the downwind side of this first series of mountains, the air subsides and creates a drier region between the Coast and the Rocky Mountains. Then, the atmospheric circulation meets a higher topographic barrier (the Rocky Mountains) and again, the air rises, condenses and precipitates on the upwind side of the mountains resulting in a second band of precipitation maximum along the boundary of British-Columbia and Alberta (Fig. 3). This second band of maximum is less intense than the first one since the air has already lost some of its humidity through the journey. East of the Rocky Mountains, dry conditions prevail. Both simulations W15 and W45 reproduce the southwesterly flow over the region as can be seen in Figure 4, which shows the mean sea level pressure as well as the horizontal wind speed and direction. Moreover, both simulations capture well the climatological pattern of precipitation (Fig. 5a-b). Of course, differences exist between the two simulations as the 15-km total precipitation rate tends to be overall larger than the 45-km precipitation (3.63 mm/day vs 3.32 mm/day). The two bands of precipitation maximum are defined better in the 15-km run than in the 45-

km run. The annual cycle shows that most of the precipitation falls during the cold months (October to March; Fig. 5c) which is in line with the observed climatology.

When looking at RCM simulations, it is important to keep in mind that the ability of the model to reproduce the observed climatological pattern is greatly influenced by its own topography. The model topography is sensitive to the horizontal resolution as it can be seen on Figure 6 where the 45-km and the 15-km topographies are shown. In the 15-km simulation, the "true" topography is averaged over an area of 225 km^2 compared to an area of 2025 km^2 in the 45-km simulation. This means that less topographic details (mountains, hills and valleys) are lost through the process of averaging in the 15-km simulation than in the 45-km simulation (Fig. 6). This leads to a more realistic topography in the 15-km simulation than in the 45-km simulation.

For example, the CRCM 15KM topography (Fig. 6a) shows peaks in northern Washington state (USA) ranging between 1000 m and 1400 m, in the Olympic National Park (with its highest point being Mount Olympus at 2500 m high in reality). However, the CRCM 45KM topography (Fig. 6b) shows a much smaller peak at about 300 m high. The presence of the Olympic National Park Mountains plays an important role on the climate of the surrounding region and the differences between the 15-km and the 45-km topography results in significant differences on the precipitation field over the region. The persistent southwesterly flow of humid air meets the mountains and creates abundant precipitation Southwest of the park and drier conditions northeast of it. Located on the leeside of these mountains, Victoria Int'l Airport (BC, Canada) receives 783 mm of precipitation per year in average and precipitation occurs[1] 138 days/year[2] (Table 4.1). Only 150 km northeast of Victoria, the city of Vancouver (BC, Canada) experiences a much wetter climate since it is located on the upwind side of the Coastal Range. The annual precipitation amount observed

[1] In this study, whenever we are referring to the number of days with precipitation (also called number of wet days), we are referring to the number of days with at least 0.2 mm of precipitation.
[2] Based on the Environment Canada's hourly-precipitation network of weather stations used in this study, see section *3.2* for more details.

at North Vancouver Sonora Dr is 1975 mm and the number of wet days is 163 days/year[3] (Table 4.1). North Vancouver Sonora Dr receives about twice the amount received in Victoria and there is 20% more rainy days in Vancouver than in Victoria.

The amount of simulated precipitation at the closest grid point of Victoria Int'l Airport in the CRCM 15KM is 1264 mm/year and it precipitates 166 days/year (Table 4.1). The 45KM simulation generates 1409 mm/year of precipitation over 198 days/year (Table 4.1). For the Vancouver area, both simulations' topography depicts the Coastal Range even though there are more details at 15-km that at 45-km. As a result, the two simulations generate comparable, but higher than observed, values of annual precipitation at the closest grid point of North Vancouver Sonora Dr. The 15-km simulation generates an annual precipitation amount of 2865 mm and precipitation occurs 175 days/year (Table 4.1). The 45-km simulation produces 2516 mm/year of precipitation and it happens 212 days/year (Table 4.1). The precipitation amount ratio Vancouver/Victoria is 2.5 in the observations while it is 2.3 for the 15-km simulation and 1.8 for the 45-km simulation. In other words, both simulations reproduce a drier climate for Victoria than for Vancouver and both of them agree that precipitation falls more often over Vancouver than Victoria like in the observations. However, within the 45-km simulation, the difference in precipitation amount between Victoria and Vancouver is somehow incorrect. The 45-km annual precipitation amount for Vancouver is less than twice the amount for Victoria. However, the 15-km annual precipitation amount for Vancouver is about twice the amount for Victoria, which is more in agreement with observations (Table 4.1).

The incorrect precipitation ratio between Victoria and Vancouver highlights an important characteristic of the 45-km precipitation resulting from the weaker precipitation gradient in the W45 simulation than in the W15 simulation (Fig. 7). The 45-km precipitation (Fig. 7b) is almost uniform between the Olympic National Park and Victoria, which are about 150 km apart. To the northeast of Victoria, the precipitation in the 45-km simulations starts to gradually increase in direction of Vancouver. In the 15-km simulation (Fig. 7a) however, the

[3] Based on the Environment Canada's hourly-precipitation network of weather stations used in this study, see section *3.2* for more details.

Southwest-Northeast precipitation gradient in the area is stronger than in the 45-km simulation. In fact, the 15-km precipitation captures clearly the rain-shadow area between the Olympic National Park and Vancouver where Victoria is located.

The latter aspects allow us to understand that the choice of grid point used for comparison with the weather stations might affect the subsequent results. In order to compare model data with observations, we use in this study the closest grid point to the weather station (see section *3.3*). However, this does not mean that the closest grid point is the most representative grid point to the weather station. What we mean by most representative grid point is a grid point whose surrounding topography is similar to the real topography around the weather station. For example, if a weather station is located at the bottom of a deep valley, the most representative grid point to that weather station should also be located at the bottom of a valley. Because of horizontal resolution though, the valley in the model may not be as deep as in reality or the model valley could be shifted from the real location of the valley, which may make the closest grid point not the most representative one. With the example of Victoria and Vancouver mentioned above, it turns out that the closest grid point of Victoria Int'l Airport is also the most representative one for both simulations. However, the closest grid point of North Vancouver Sonora Dr is not the most representative grid point for both simulations. Indeed, for the two simulations the closest grid point is in the slope of the mountain (Coastal Range) meaning that the altitude of the closest grid point is too high compared to the altitude of the weather station (Table 4.2) and located in a location with more precipitation (the upslope region). The most representative grid point of North Vancouver Sonora Dr was picked within a one grid point radius of the closest grid point (for both simulations) and is located at the bottom of the mountain (Table 4.2). Using the most representative grid point instead of the closest grid point doest not change the main conclusions mentioned earlier, but it does have an effect. For instance, with the most representative grid point, the 15-km ratio between the Vancouver and Victoria annual precipitation amount is now of 2.5 which is equal to the observed ratio. On the other hand, the 45-km run shows a ratio of 1.3 which is even further away from observations than it was with the closest grid point (Table 4.1). This shows that because the model tries to reproduce a regional climate on a three-dimension grid with finite resolution (horizontal and vertical), the

results are sensitive to the grid point used for comparison. To simplify the comparison between model and observations though, we will use the closest grid point to the weather station as explained in section *3.3*.

4.1.2 Analysis of the water cycle components

The previous results show that the more realistic topography found in the 15-km simulation seems to lead to a better spatial distribution of precipitation, especially in valleys or on the lee side of mountains. On the other hand, the simulation W15 produces globally more precipitation than the simulation W45. Why and how is this humidity generated in the simulations? To answer these questions, we analyzed the contribution of the different components of the hydrological cycle to the total precipitation. We find that both simulations show convergence of humidity on the upwind side of mountains or hills, while on the downwind side of mountains divergence occurs (Fig. 8a-b). The Pacific Coast has the highest values of convergence of humidity of the entire domain. Over that area, the 15-km convergence of humidity varies from 6 to 12 mm/day (Fig. 8a) while the 45-km convergence of humidity ranges between 6 and 10 mm/day (Fig. 8b). A second less intense maximum of convergence of humidity can also be identified west of the Continental Divide, where the 15-km convergence of humidity is also greater than the 45-km one. Over those regions, most of the total precipitation comes from convergence while elsewhere on the domain, convergence and evapotranspiration (Fig. 8d-e) respectively provide about half the humidity needed to generate precipitation. Also, both runs agree that evaporation is maximal over the ocean. Between the two topographic barriers and over the prairies, large evapotranspiration rates can also be found. The lowest values of evapotranspiration appear over mountains (Fig. 8d-e). As a result, the simulations W15 and W45 both reproduce the two observed bands of precipitation maximum (see Fig. 3) west of the Coastal Range and west of the Rocky Mountains (Fig. 8g-h).

Because the simulation W15 produces globally more convergence of humidity and evapotranspiration than the simulation W45, the 15-km total precipitation (Fig. 8g) is larger

than the 45-km total precipitation (Fig. 8h). This latter fact is especially true along the Coastal Range since the 15-km precipitation ranges between 9 to 15 mm/day while the 45-km precipitation ranges between 5 to 10 mm/day. It is also found that the two simulations agree that the highest convergence of humidity is found from November to March (Fig. 8c), which corresponds the wettest period of the year (Fig. 8i). In fact, during the winter, most precipitation comes from convergence of humidity brought by many of the low pressure systems coming from the Pacific Ocean. During summer though, about two thirds of the precipitation comes from evapotranspiration (Fig. 8f). However, the minimum of precipitation is reached during the warm season. Being the warmest period of the year (Fig. 9c), summer time enhances the conversion of evapotranspiration into convective precipitation. Globally, the simulation W15 is cooler of about 0.3°C than the simulation W45 (Fig. 9a-c). However, it seems that 15-km surface temperature is lower than the 45-km surface temperature during the cold months of the year (November to March; Fig. 9c). Also, the 15-km simulation is cooler than the 45-km simulation over the northern section of the WEST CAN domain (Yukon and North-West Territories) as well as over the mountainous regions (Coastal Range, Rocky Mountains and Olympic National Park; Fig. 9a-b). The mean annual cycle of surface temperature (Fig. 9c) also reveals that both simulations agree that the surface temperature remains above freezing from April to October. As a result, almost all of the total precipitation falls as liquid during those months (Fig. 9f). In fact, over the WEST CAN domain most of the total precipitation falls in its liquid form. As it can be seen in Figure 9d-f, liquid precipitation contributes respectively to 80% and 78% of the total precipitation within the 15-km and 45-km simulations. Moreover, the 15-km liquid precipitation is greater by about 0.3 mm/day than the 45-km liquid precipitation, and especially on the upwind side of the Coastal Range (Fig. 9d-e). From December to March, some of the precipitation falls as solid form (Fig. 9i) and both simulations agree that most of that solid precipitation falls over the Coastal Range and over the Rocky Mountains (Fig. 9g-h). Over those areas, the 15-km solid precipitation is greater than the 45-km solid precipitation while over the Alberta prairies the opposite is seen. This leads to a 15-km simulation that produces globally about 0.01 mm/day less solid precipitation than does the 45-km simulation. Since solid precipitation represents only about 20% of the total precipitation, the 15-km total precipitation remains higher than the 45-km total precipitation.

In addition to solid precipitation, it is also interesting to look at the water equivalent of snow on the ground. The two simulations agree that the snow water equivalent is maximal over the northern section of the domain and over the mountains, with values above 200 mm (Fig. 10a-b). This makes sense since we have seen earlier that those regions are the ones receiving the more snow (Fig. 9g-i). Over those regions though, the 15-km snow water equivalent is greater than the 45-km one (Fig. 10a-b). Over the Alberta prairies, the lower 15-km solid precipitation leads to a lower snow water equivalent (especially over northern Alberta), compared with the 45-km snow water equivalent. As a result, the domain average of snow water equivalent is superior within the simulation W15 than within the simulation W45. On a yearly basis, it is noticeable that the amount of snow water equivalent produced by both simulations is of about 200 mm at the end of the winter (Fig. 10c). The 15-km simulation snow water equivalent remains slightly greater than the 45-km one during spring and summer (Fig. 10c). This can be explained by the following. Because the 15-km simulation is cooler than the 45-km simulation, snow takes slightly more time to melt in the higher resolution simulation, which explains the difference in snow water equivalent during spring. Moreover, because of the finer horizontal resolution, the 15-km run is able to simulate some of the permanent snow present at the top of the highest mountains, which keeps the 15-km snow water equivalent slightly above 0 mm during the summer months (Fig. 10c). The latter fact explains why the snow water equivalent is globally greater within the 15-km run than within the 45-km run even though the 15-km solid precipitation is inferior to the 45-km solid precipitation. Since the maximum of runoff is directly linked to the melting of snow and that the solid precipitation is little bit inferior at 15 km than at 45 km, the maximum of runoff (in April) is lower in the simulation W15 (Fig. 10f). Over the entire domain, the 15-km runoff is inferior to the 45-km runoff, with a respective domain-averaged runoff of 1.63 mm/day and 1.79 mm/day (Fig. 10d-e). However, both simulations agree that there is more runoff along the Pacific coast associated to the region with the largest precipitation. Moreover, we have seen that the evapotranspiration is superior for the 15-km simulation than for the 45-km one over most of the domain and especially during the warm months (Fig. 8d-f). Therefore, more surface water can be evaporated which also reduce the runoff in the 15-km simulation with respect to that at 45-km.

In summary, the 15-km simulation produces more precipitation than the 45-km simulation, mostly resulting from the larger convergence of humidity in the 15-km simulation than in the 45-km simulation, especially along the Pacific Coast. The greater 15-km convergence of humidity found along the coast is explainable by higher 15-km topography over the area (see Fig. 6). Furthermore, figure 9a-b reveals that both simulations reproduce a low pressure system over the Pacific Ocean. Within the simulation W15, this low-pressure system generates more than 350 wet days per year, which is about 25 more days than what the simulation W45 generates (Fig. 10g-h). In other words, it rains more often in the 15-km run than in the 45-km run over the Pacific Ocean. Thus, more humidity (coming from this low) can be transported towards the coast, which is another reason why the convergence of humidity along the coast is greater within the 15-km simulation than within the 45-km simulation. Over the continent, both simulations agree that the number of wet days is greatly correlated with the topographic features: 1) precipitation occurs more often on the upwind side of topography, and 2) precipitation is less frequent within the valleys and on the lee side of mountains (Fig. 10g-h). Because of a more realistic topography, this variable is better defined within the 15-km simulation. In fact, the number of wet days west of mountains and hills is greater in the simulation W15 than in the simulation W45 (Fig. 10g-h). On the lee side of mountains and hills, the number of wet days seems lower within the 15-km run than within the 45-km run (Fig. 10g-h). When looking globally, it seems that the number of wet days is lower at 15-km than it is at 45-km, which can be seen with the domain average of this variable (Fig. 10g-h) as well as with the annual cycle (Fig. 10i).

4.2.3 Comparison between model and observations

Until now, we have seen that the 15-km simulation produces more precipitation than the 45-km simulation. It also appears that the simulated precipitation is larger than the observed precipitation in both simulations, at least at the two weather stations mentioned above. The wet bias is also true according to the mean annual cycle of precipitation obtained with all the 27 weather stations of the Environment Canada's hourly precipitation network for the WEST CAN domain (Fig. 11). The difference between simulated monthly precipitation and observed monthly precipitation is about 1.7 mm/day (52 mm/month) for the simulation W15 and about 1.1 mm/day (33 mm/month) for the simulation W45. The 15-km precipitation is systematically greater by about 0.6 mm/day (18 mm/month) than the 45-km precipitation. However, the two simulations correctly capture the fact that the greater precipitation occurs between October and March, and that the lower precipitation arises throughout April to September.

As mentioned previously, the CRCM simulated precipitation (in both simulations) is greater than the observed precipitation. At this point, it would be important and interesting to know why the simulated precipitation is systematically greater than the observation. To answer this question, one has to seek beyond what is revealed through the annual cycle. The annual cycle is good to reveal differences in precipitation amount, but it does not indicate what type of precipitation event (light, moderate, heavy or very heavy) is the main source of the total amount. To get that kind of information, we have to analyse the precipitation frequency (PF) and precipitation intensity (PI) for different precipitation events (PE). In the following, we then concentrate our analysis on those precipitation features. Following the recommendations of Trenberth (1999; 2003), hourly precipitation data is used to analyse the PF and PI. As pointed out in Gutowski Jr. et al (2003), the most intense PE (heavy and very heavy) generally occur within an hour, which then makes hourly precipitation data more appropriate for the frequency and intensity analysis. Using the hourly accumulation period, we created observed and simulated histograms (Fig. 12). Observed and simulated PF distributions display that as the intensity of hourly PE (HPE) increases, the frequency

decreases (Fig. 12a). The distributions also reveal that the frequency of 0-0.2 mm/h HPE is about 10% inferior within the two simulations than for observations. In section *3.3*, we mentioned that the common threshold for the simulated and observed precipitation was 0.2 mm/h, which means that 0-0.2 mm/h HPE (hereafter trace HPE) represent events with no precipitation. Thus, the previous result can also be interpreted as follows: precipitation occurs 10% more often in the model than what is observed. Within both simulations, this exceeding 10% can be attributed to light HPE (0.2-3 mm/h). As a result, both simulations produce more light HPE than observed which is typical of climate models (Mearns et al. 1995; Chen et al. 1996; Giorgi and Marinucci 1996; Gutowski Jr. et al. 2003). In fact, the 15-km PF and 45-km PF of light HPE is respectively of 19% and 22% which is about twice the observed PF of 10%. On the other hand, the two simulations agree with observations that most of the precipitation occurs with those HPE (Fig 12c). The remaining precipitation comes from moderate (3-6 mm/h), heavy (6-10 mm/h) and very heavy (>10 mm/h) HPE. However, the 45-km PF starts to fall rapidly below the observed PF for events greater than 3 mm/h (moderate HPE) and reach 0% for events greater than 6.4 mm/h (heavy and very heavy HPE). For example, the simulation W45 produces five times less 5-mm/h events than observed, while the 15-km PF is slightly superior to the observed PF for events between 3 mm/h and 8.6 mm/h (moderate HPE and most heavy HPE). The simulation 45-km PF is also is inferior to the observed PF for events greater than 8.6 mm/h. For instance, the very heavy HPE (>10 mm/h) occurs about 0.14% less often within the 15-km simulation than observed. Contrarily to the 45-km simulation, the 15-km simulation is thus able to reproduce HPE of all kind: from synoptic system (light and moderate HPE) as well as from the intense but short convective events (moderate to very heavy HPE). As a result, the 15-km PF distribution is more realistic than the 45-km PF distribution.

Since any HPE is characterised by space and time, it is imperative to learn more about the spatial frequency of observed and simulated precipitation. The spatial frequency of precipitation can be seen in Figure 12b. In effect, the observed distribution indicates the number of weather stations (y-axis), among the 27 used for analysis, where a given HPE occurs (x-axis). To its turn, the model distributions indicate the number of grid points (y-axis), among the 27 used for analysis, where a given HPE occurs (x-axis). For example, 3

mm/h HPE occurs at all the 27 weather stations and all the 27 15-km grid points, but only at 25 of the 27 45-km grid points. At first sight, the distributions reveal that moderate to very heavy HPE are more localised in space than trace and light HPE. Moreover, moderate to very heavy HPE are more localised within the model than they are in reality, meaning that the model creates less moderate to very heavy HPE than what is observed. This is particularly true for the simulation W45. Because of lower horizontal resolution, there are less 45-km grid points than there are weather stations with moderate to very heavy HPE. With a higher horizontal resolution though, the 15-km simulation is able to reproduce all the types of HPE at some of its grid points (among the 27 used for analysis).

As mentioned earlier, the PI is another important feature of precipitation that needs to be analysed. The analysis reveals that the intensity of light and moderate HPE is about 0.04 mm/h greater for both simulations than for observations (Fig. 12c). For heavy HPE, the 15-km intensity is about the same as observed while for very heavy HPE (>10 mm/h), the 15-km intensity is 1.6 mm/h inferior to the observed intensity. To its turn, the 45-km PI for heavy and very heavy HPE is incorrect because the simulation produces no such HPE (see Fig. 12a-b). So, the 15-km PI distribution is more realistic than the 45-km PI distribution.

In terms of time frequency (Fig. 12a), spatial frequency (Fig. 12b), and intensity (Fig. 12c) of simulated precipitation, both simulations produce more precipitation annually than observed (Fig. 12d). The total annual precipitation amount (APA) observed is of 1032 mm compared to a total APA of 1635 mm and 1411 mm for the simulations W15 and W45, respectively. Most of the excess in precipitation (compared to observations) within the model comes from light HPE. Those events produce 1215 mm and 1286 mm annually within the 15-km and 45-km simulations, which is almost twice the observed amount of 667 mm. For moderate HPE, the 15-km APA is 46 mm greater than the observed amount while the 45-km APA is 138 mm inferior to the observed amount. Of course, since the 45-km simulation produces no heavy and very heavy HPE, the amount produce by those events is zero. On the other hand, the 15-km simulation produces about 30 mm more precipitation than observed with heavy HPE. The very heavy HPE contribute to only 3 mm annually within the 15-km simulation, which is 20 mm below the observed amount. Because the 45-km simulation

generates much less precipitation than observed with moderate to very heavy HPE, this compensates for the excess in precipitation produced by light HPE. Within the 15-km simulation though, there is no compensation between light HPE and moderate to very heavy HPE. So, if one was to look only at the total annual precipitation, one might think that the 45-km is more in agreement with observations than is the 15-km simulation. However, we have seen in Figure 12 that the 15-km hourly distributions are more realistic than the 45-km distributions. In other words, the 45-km total annual precipitation may be closer to the observed value but this comes from a wrong PF and PI distributions.

The previous analysis was made on hourly accumulation period. According to Trenberth (1999; 2003), climate change should lead to an augmentation of heavy precipitation events as well as an increase in the frequency of droughts. In those studies, it is also suggested that hourly precipitation data should be used to analyze the precipitation frequency and intensity since it better fits the lifetime of heavy and very heavy precipitation. However, it is frequent that daily precipitation data are used to fill this task. As Gutowski Jr. et al. (2003) explains, the problem with using a daily accumulation period is that the short bursts of convective precipitation are smoothed by the time averaging. Also, a very strong PE is usually not sustained for an entire day. The impact of this is better explained with an example. Let us suppose that on a hot and humid summer day, diurnal convection forms during afternoon and that a heavy HPE occurs and gives 8 mm/h at a given weather station. After the shower, the sky becomes clear again and no more precipitation falls at the station for the rest of the day. So, this event will be the only one to contribute to the total daily accumulation (8 mm/day). Let us now suppose another scenario in which an organized low pressure system passes over the same weather station. At the passage of the warm front, steady precipitation is falling to the rate of 2 mm/h (light HPE). Once the warm front has passed the weather station, 4 hours of precipitation have been recorded with a total of 8 mm. If it does not precipitate more during the day, those 8 mm will contribute to a similar total daily accumulation (8 mm/day). So, if the PF or the APA distribution was obtained with a 24-h accumulation period, those two events (convective versus synoptic) would not show any differences. For that reason, using a 24-h accumulation period to create the PF and the APA distributions introduces changes in the results.

As we did with an hourly accumulation interval, we created simulated and observed histograms for a daily accumulation period (Fig. 13). The daily PF histogram displays that as the daily amount increases, the frequency decreases (Fig. 13a). In effect, the three distributions show that the frequency of light daily PE (DPE; 0.2-10 mm/day) is around 30% while the frequency of very heavy DPE (> 40 mm/day) drops to about 1%. The daily PF histogram also reveals that both simulations reproduce quite equally the observed PF distribution. However, the 15-km and 45-km PF are respectively greater of about 1.56% and 1.49% than the observed PF for all intensity classes except dry days (0-0.2 mm/day). Dry days account respectively for 49% and 48% of the time within the 15-km and 45-km simulations, which about 10% inferior to what is observed. This means that precipitation occurs more often within the model than in reality (as we also saw with hourly histograms in Fig. 12). Within the two simulations, this excess in occurrence of precipitation is then quite evenly distributed throughout light DPE (0.2-10 mm/day), moderate DPE (10-20 mm/day), heavy DPE (20-40 mm/day), and very heavy DPE (> 40 mm/day). Nevertheless, the major difference between the two simulated PF distributions is found at both ends of the distribution, that is light DPE and very heavy DPE. For light DPE, the simulation W15 is slightly closer than the simulation W45 to the observed PF. For the very heavy DPE though, the 45-km PF is closer to the observed PF with a bias (simulated - observed) of 0.2% compared to a bias of 1.2% for the 15-km simulation. Even if the 45-km hourly PF distribution did not follow the observed hourly PF distribution (Fig. 12a), it reproduces (even slightly better than the 15-km run) the observed daily PF distribution. This can be explained by the fact that the heavy and very heavy HPE (> 6 mm/h) that the 45-km simulation does not produce are very rarely observed (about 0.1% of the time; Fig. 12a), and then do not often contribute to increase the daily amount. The events that do contribute to increase the daily amount are those generated by synoptic systems, that is light to moderate HPE (0.2-6 mm/h). Since the 45-km simulation produces more light HPE than observed and generates less moderate HPE than observed, there is compensation between the two types of events. This results in a slightly more realistic daily PF distribution. On the other hand, the 15-km simulation, which showed a more realistic hourly PF distribution, produces more light HPE than observed as well as slightly more moderate to heavy HPE than observed. The impact is

that the two types of PE do not compensate each other and then, the 15-km daily PF distribution does not seem better than the 45-km daily PF distribution.

The spatial frequency histogram (Fig. 13b) shows that the heavy and very heavy DPE are more localized than the light DPE. The histogram also demonstrates that the two simulated distributions are similar to the observed one. A similarity is also found between the simulated and observed daily PI distributions shown in Figure 13c. The major difference resides with days producing more than 49 mm of precipitation, where the 15-km simulation is closer than the 45-km simulation to the observed PI.

As a result of the time frequency (Fig. 13a), the spatial frequency (Fig. 13b), and intensity of precipitation (Fig. 13c), the total observed and simulated APA is provided quite equally by light DPE to very heavy DPE (Fig. 13d). In fact, the observed distribution shows that light DPE are responsible for only 292 mm of precipitation annually, which is about the same as the annual contribution of moderate DPE (267 mm/year) and heavy DPE (278 mm/year). Very heavy DPE contribute slightly less to the annual total with a 195 mm of precipitation. Those results demonstrate that it takes many more light DPE to accumulate the same amount that only few moderate DPE can create. The APA histogram also display a 15-km APA and a 45-km APA greater than the observed APA for all intensity classes, with the 15-km APA distribution remaining though slightly closer to the observed distribution for any days with less than 49 mm/day. Within the 15-km simulation, days with at least 49 mm contribute to about twice the observed amount, which is not the case within the 45-km simulation.

4.2 EAST CAN domain

4.2.1 Analysis of the water cycle components

Contrarily to the WEST CAN domain, the eastern part of Canada (EAST CAN domain) has a much flatter terrain. As a result, topography plays a less important role in the formation of precipitation. The differences in the topography between the 15-km and 45-km simulations are not as obvious as they are over the WEST CAN domain. However, the E15 topography (Fig. 14a) shows finer details than the E45 topography (Fig. 14b). For example, both the 15-km and 45-km simulations depict their tallest grid point over the Réserve Faunique des Laurentides (Qc, Canada), with a height being between 800 m and 900 m at 15 km and between 700 m and 800 m at 45 km. The W15 height is then closer to the tallest peak of the region which exceeds 1000 m in reality. Moreover, the Réserve Faunique des Laurentides topography is better defined within the 15-km run than it is within the 45-km run. There are some other mountainous regions that are better resolved at 15 km than at 45 km, such as the Monts Chics-Chocs in Gaspésie (Qc, Canada) and the Adirondack National Park (NY, USA). The St-Lawrence and Richelieu valleys are also better represented in the 15-km simulation. The differences in topography between the simulations E15 and E45 lead to some differences in the convergence of humidity field (Fig. 15a-b), which to its turn leads to differences in the precipitation field (Fig. 15g-h). In effect, the 15-km convergence of humidity (Fig. 15a) is greater than the 45-km convergence of humidity (Fig. 15b) mainly on the upwind side of the Adirondacks (NY, USA), but also along the coast of Nova Scotia (Canada) and over the South coast of Newfoundland (Canada). As a result, the 15-km convergence of humidity is globally greater of about 0.17 mm/day than the 45-km convergence of humidity (Fig. 15a-c). Both simulations do agree though with the location of the maximum of convergence. In effect, the convergence of humidity is highly correlated with the topography, and it is greater on the upwind side of mountains or hills as well as along coastal regions and it is lower over valleys (Fig. 15a-b). The two simulations also agree that the evapotranspiration is greater over the southern section of the domain (Fig. 15d-e) due to the highest surface temperature found there (Fig. 16a-b). Also, the maximum of evaporation is found over the Gulf Stream Current. Overall, the 15-km simulation produces about 0.11 mm/day more evapotranspiration

than does the 45-km simulation, and the 15-km evapotranspiration is especially higher than the 45-km evapotranspiration over the Great Lakes and over the Gulf Stream Current (Fig. 15d-e). As a result, the simulation E15 generates about 0.27 mm/day more precipitation than does the simulation E45 (Fig. 15g-i). The 15-km precipitation is particularly greater than the 45-km precipitation East of Lake Erie and Lake Ontario, probably meaning that the lake effect on snow is more important in the 15-km run than in the 45-km run. The 15-km precipitation is also higher than the 45-km precipitation over the Adirondacks and Appalachians mountains, as well as along the coast of Nova Scotia and the South coast of Newfoundland (Fig. 15g-h).

Thus, over the EAST CAN domain precipitation is generated by convergence of humidity or by evapotranspiration. The contribution of each source of humidity to the total precipitation mainly depends on the time of the year (Fig. 15). In fact, the synoptic activity starts to increase in intensity in September as the jet-stream begins to move southward, then meaning that the trajectory of depressions also move southward. Then, most precipitation during fall is generated trough low pressure systems that enter the domain from the South border or the West border. As mentioned earlier, these lows can come from different locations with the most well known locations being: Alberta (Alberta Clipper), Colorado (Colorado low), Gulf of Mexico, and Cap Hateras or East coast of USA (Cap Hateras low or Coastal low; Zishka and Smith 1980). As a consequence, lots of humidity is brought into the region through advection during the months of September, October and November (which is visible with the convergence of humidity displayed in Fig. 15c). In fact, both simulations agree that during the fall season, the convergence of humidity reaches a first maximum (Fig. 15c). This maximum of convergence, that account for two third of the total precipitation, added to the evapotranspiration, that is still quite important during that period of the year (Fig. 15f), makes the fall season the wettest of the year (Fig. 15i). In addition to the south displacement of the jet stream that starts in autumn, autumn also corresponds to the hurricane season over North America, which helps making it the wettest period of the year. Forming over the warm tropical water of the South Atlantic, some of these hurricanes (as hurricane or as extratropical cyclone) follow a North-East trajectory and generate lots of precipitation over the EAST CAN domain. During the winter season, both simulations agree that less humidity

is condensed in the region (Fig. 15c) and less evapotranspiration is created as well (Fig. 15f) which makes it the driest season of the year (Fig. 15i). This can seem quite a surprise knowing that during the winter season many snow storms hit the provinces of Quebec and Ontario; this minimum of precipitation can be explained by the following. During winter, temperature generally remains below freezing (Fig. 16c) which then makes most precipitation to fall in solid form (Fig. 16i). When a snow storm hits the domain, great amount of snow can be produced. However, great amount of snow does not necessarily mean great amount of water. Indeed, 10 cm of snow can be equivalent to as much as 10 mm of water, but it can also be equivalent to only 2 mm of water. The provenance of the low pressure systems dictates the snow water contain. In effect, Alberta Clippers and Colorado lows have a small snow water contain while the Gulf of Mexico and Cap Hetaeras lows have a much larger snow water contain. During the spring season, the convergence of humidity reaches another maximum (Fig. 15c) but the total precipitation during that season remains below the amount received during fall (Fig. 15i). This is mainly explainable by the fact that during spring, the evapotranspiration is smaller than it is during autumn (Fig. 15f). Indeed, up to the month of October, most of the trees still have their leaves on, which then contributes to increase the evapotranspiration. On the other hand, the leaves generally do not start growing back on trees before May, which helps maintaining the evapotranspiration low during the spring. The second maximum in total precipitation is reached during the warm season (Fig. 15i). Contrarily to the autumn though, during summer both runs simulate a maximum of evapotranspiration (Fig. 15f) due to a surface temperature that is maximal and above freezing (Fig. 16c). In fact, more than two third of the total precipitation comes from evapotranspiration during summer (Fig. 15f), and all of that precipitation is in liquid form (Fig. 16f). It is not surprising to see that a second maximum of precipitation is reached during summer because convective activity is more intense. Due to the warm and humid air present in the environment, convective systems (from the individual cells to the cells embedded along a cold front) can form and generate intense but short burst of precipitation (Gutowski Jr. et al., 2003). Over the entire domain, both simulations agree that liquid precipitation represent about 75% of the total precipitation. The two simulations also agree that liquid precipitation is greater in the South-East section of the domain (Fig. 16d-e) which follows the South-East to North-West surface temperature gradient (Fig. 16a-b). The solid precipitation

field (Fig. 16g-h) shows a South-West to North-East gradient with the larger rate found over northern Labrador (NL, Canada) and East of the Ungava Bay (QC, Canada). A local maximum of solid precipitation is also found in both simulations over the Réserve Faunique des Laurentides (QC, Canada; Fig. 16g-h). However, the 15-km solid precipitation over those regions as well as over other mountainous regions (the West coast of New-Found Land for example) is larger than the 45-km solid precipitation, resulting from the higher elevation (because of a better defined topography) at 15 km than at 45 km. Another interesting difference between the two simulations resides over some of the Great Lakes. The 15-km simulation produces more solid precipitation than does the 45-km simulation East of Lake Superior, Lake Erie, Lake Ontario, and East of the Georgian Bay (ON, Canada). The lake snow effect is more intense and better resolved (a local phenomenon) within the 15-km run than within the 45-km run.

Despite agreeing on the timing and location of solid and liquid precipitation, the two simulations show important differences in values. In effect, the simulation E15 produces about 0.25 mm/day more liquid precipitation than does the simulation E45 (Fig. 16f). The largest difference in liquid precipitation occurs from June to October, which corresponds the wettest period of the year (Fig. 15i). However, the 15-km solid precipitation globally resembles the 45-km solid precipitation since the domain averaged of this variable is respectively of 0.65 mm/day and 0.64 mm/day (Fig. 16g-h). When looking at the snow water equivalent simulated by both simulations, we realize that the 15-km simulation shows a slightly greater snow water equivalent than does the 45-km simulation (Fig. 17a-b). The two simulations do agree on the location of the larger snow water equivalent amount in the domain over the eastern and north-eastern portion of Quebec and Labrador (Fig. 17a-b). They also agree that the peak of snow water equivalent is reached in March, with a slightly higher maximum at 15-km than at 45-km (Fig. 17c). As a result of a greater precipitation and snow water equivalent in the 15-km simulation, the surface runoff is superior for the 15-km simulation than for the 45-km simulation (Fig. 17d-f). This is especially true from May to December (Fig. 17f). In May, most of the snow has melted which explains the maximum in runoff reached for this month for both simulations (Fig. 17f). Since the snow water equivalent and precipitation is greater at 15 km than at 45 km, the surface runoff remains

greater for the 15-km run than for the 45-km run during the spring (Fig. 17f). During summer and fall, the 15-km runoff remains greater than the 45-km runoff only because the 15-km precipitation is superior to the 45-km precipitation (Fig. 15i). Over the domain, both simulations reproduce the maximum of runoff at the same locations: east of the Ungava Bay, east of Lake Ontario, south-east of Lake Erie, over the Adirondacks, over the Appalachians, and along the South coast of Newfoundland (Fig. 17d-e). In other words, the runoff is greater near mountains as well as near large bodies of water (lakes, gulf and ocean). However, at all these locations an then globally over the entire domain, the 15-km runoff is 0.09 mm/day superior to the 45-km runoff (Fig. 17d-e).

In summary, the 15-km simulation produces more precipitation than the 45-km simulation, which can be attributed to a greater 15-km convergence of humidity mostly during fall and a greater 15-km evapotranspiration mostly during summer. Since summer and autumn are the two wettest season of the year, the difference in humidity between the two simulations during those seasons contribute the most to the difference in precipitation. Moreover, these two seasons experiment more days with precipitation (Fig. 17i). Indeed, the number of wet days per month during summer is about 22 within both simulations, and this number goes to about 24 during fall. We can also notice that on average, the number of wet days is superior within the simulation E15 than within the simulation E45 (Fig. 17g-i). This is especially true from August to March (Fig. 17i) and East of Lake Erie and Lake Ontario, over the Gulf Stream Current and west of Newfoundland and Cape Breton Island. We can notice that the sharper 15-km topography leads to more wet days on the upwind side of mountains. Moreover, it is noticeable that the places with a high number of wet days match with the places receiving more precipitation (Fig. 15g-i). Overall, it precipitates more often within the simulation E15 than within the simulation E45, which can explain partially why the 15-km precipitation is greater than the 45-km precipitation.

4.2.2 Comparison between model and observations

Until now, we have found that the 15-km simulation produces more precipitation than does the 45-km simulation for every month of the year. According to the observations coming from the 45 weather stations of Environment Canada's hourly precipitation network for the EAST CAN domain, this means that the 15-km precipitation is generally greater of about 0.2 mm/day (6 mm/month) than the observed precipitation (Fig. 18). The 45-km precipitation is generally smaller by about 0.1 mm/day (3 mm/month) than the observed precipitation (Fig. 18). Both simulations reproduce the shape of the annual cycle, with the wettest period extending from July to November (summer and fall). However, the two simulations produce more precipitation than observed during spring and fall. During summer, it seems that the simulation E15 generates more precipitation than observed while the simulation E45 does produce less. For December and January, both runs simulate less precipitation than observed while for February and March, they reproduce quite well the observed precipitation. The analysis of the water cycle components for the EAST CAN domain highlighted the following fact. The 15-km simulation produces more precipitation than the 45-km simulation, and that can be attributed to a greater 15-km convergence of humidity during fall and a greater 15-km evapotranspiration during summer. So, this would suggest that the convergence of humidity is responsible for the greater precipitation than observed seen for both simulations during spring and fall (see Fig. 15a-c). During summer, the difference in evapotranspiration between the two simulations would explain the difference seen with observations (see Fig. 15d-f). This could imply that due to a greater evapotranspiration, the 15-km simulation produces more convection during the warm months of the year (compared to the 45-km simulation), which leads to more precipitation than observed.

In order to clarify the reasons explaining the difference between simulated and observed precipitation, we computed simulated and observed histograms of PF and PI for an hourly accumulation interval (Fig. 19). Observed and simulated PF distributions display that as the intensity of Hourly Precipitation Event (HPE) increases, the frequency decreases (Fig. 19a).

The distributions also reveal that the two simulations generate about 13% of light HPE (0.2-3 mm/h), which more than twice the observed PF of 6%. The last result is typical of climate models (Mearns et al. 1995; Chen et al. 1996; Giorgi and Marinucci 1996; Gutowski Jr. et al. 2003). On the other hand, the two simulations agree with observations that light HPE are the most frequent. Indeed, the remaining precipitation (less than 1%) comes from moderate (3-6 mm/h), heavy (6-10 mm/h) and very heavy (>10 mm/h) HPE. The 45-km PF begins to fall below the observed PF for events greater than 3 mm/h (moderate HPE) while the 15-km PF remains closer to the observed PF. As a result, moderate, heavy and very heavy HPE account respectively for 0.3%, 0.02% and 0.0005% within the 45-km simulation compared to an observed PF of 0.7%, 0.15% and 0.07%, respectively. On the other hand, the 15-km PF for moderate, heavy and very heavy HPE is respectively of 0.5%, 0.07% and 0.01%, which is closer to the observed PF. So, the simulation E15 produces more moderate to very heavy HPE than does the simulation E45, which means that it is more capable of reproducing the short convective events. As a consequence, the 15-km PF distribution looks more realistic than the 45-km PF distribution.

The better ability of the 15-km simulation to produce more moderate to very heavy HPE is confirmed with the spatial frequency distributions of Figure 19b. As explained in the previous section, the observed distribution indicates the number of weather stations (y-axis), among the 45 used for analysis, where a given HPE occurs (x-axis). To its turn, the model distributions indicate the number of grid points (y-axis), among the 45 used for analysis, where a given HPE occurs (x-axis). For example, 10 mm/h HPE occur at 44 weather stations while they occur at 35 15-km grid points and only at 3 45-km grid points. Globally, the distributions reveal that moderate to very heavy PE are more localised in space than trace and light HPE. However, the model creates less moderate to very heavy HPE than what is observed and this is particularly true for the 45-km simulation. For example, events greater than 8 mm/h occur at less than 5 grid points within the simulation E45, which is about one third of the observed and 15-km spatial frequency.

As mentioned earlier, the PI is another important feature of precipitation that needs to be analysed. The analysis reveals that the simulated intensity of light HPE is about 0.03 mm/h

greater than the observed intensity of 1.56 mm/h (Fig. 19c). For moderate HPE, the mean PI of both simulations is about 0.05 mm/h greater than observed. For heavy HPE, the 15-km PI is still superior of about 0.03 mm/h to the observed intensity, contrarily to the 45-km PI that is 0.5 mm/h smaller. For very heavy HPE, the difference in mean intensity between observations and model keeps growing. In effect, the 15-km and 45-km PI for such events are respectively of 11.53 mm/h and 10.75 mm/h, which is much less than the observed intensity of 16.46 mm/h. On one hand, precipitation coming from low to moderate events is more intense in the model than what is observed but on the other hand, the two simulations have trouble reproducing the observed intensity of very heavy HPE, with the 15-km simulation being slightly closer to the observations.

As a result of the time frequency (Fig. 19a), the spatial frequency (Fig. 19b), and intensity of simulated precipitation (Fig. 19c), the total 15-km APA is slightly greater than the observed APA while the 45-km APA is slightly inferior (Fig. 19d). More specifically, the total 15-km and 45-km APA is respectively of 1045 mm and 936 mm compared to an observed APA of 973 mm. Both simulations agree with observations that most of the total APA comes from light HPE but the simulated amount is much greater within the model than what is observed. In effect, those events produce 825 mm (15-km) and 813 mm (45-km) annually which is almost twice the observed amount of 560 mm. The three distributions agree that the remaining precipitation comes from moderate to very heavy HPE, with the simulated amount being inferior than observed. For the moderate HPE, the simulations E15 and E45 generate respectively 166 mm/year and 112 mm/year, which is less than the observed amount of 223 mm. The scattered and sporadic heavy and very heavy HPE give respectively 94 mm and 96 mm of precipitation annually for observations. Within the model, those events contribute respectively to of 47 mm and 8 mm annually for the 15-km simulation while for the 45-km simulation, those events produce respectively 11 mm and nearly 0 mm annually. So, both simulations generate quite equally too much precipitation with light PE (compared with observations). Because the 45-km simulation does not generate much precipitation with moderate to very heavy PE, that compensates for the overestimation of precipitation accumulated with light HPE which results in a total 45-km APA slightly inferior than observed. On the other hand, since the 15-km simulation produces more precipitation than the

45-km simulation with moderate to very heavy HPE (which is more in agreement with observations), the compensation between light HPE and moderate to very heavy HPE is more subtle and this results in a total 15-km APA slightly superior than observed. So, if one was to look only at the total APA, one would think that the simulation E45 is slightly better than the simulation E15 in reproducing the observed precipitation. However, we have seen that the PF, PI and APA distributions are more realistic with the 15-km simulation than with the 45-km simulation. This highlights the advantage to work with hourly precipitation data: we can see what causes the model to diverge from the observations. The 45-km total APA may be closer to the observed value, but this comes from a less realistic PF and PI distributions (Fig. 19a-d).

The previous results were obtained using hourly accumulation period. As explained earlier (see section *4.1*), it is also interesting to see the impact of using a daily accumulation interval on frequency and intensity of precipitation. Using a 24-h accumulation period, we created the daily observed and simulated PF, PI and APA histograms (Fig. 20). The daily PF histogram display that as the daily amount increases, the frequency decreases (Fig. 20a). The PF distributions also reveal that the frequency of dry days (0-0.2 mm/day) is respectively of about 55% and 59% within the 15-km and 45-km simulations while the observed frequency is about 56%. Thus, dry days occurs more often than observed within the simulation E45 while within the simulation E15, they are slightly less frequent than observed. Nevertheless, the differences between the two simulations regarding PF are more subtle than when using an hourly accumulation period since at first sight, both simulations seem to reproduce quite equally the observed daily PF distribution. When looking more carefully, the 45-km PF distribution shows that light Daily Precipitation Events (DPE; 0.2-10 mm/day) are about 3% below the observed PF of 36%, which mostly explains the lower frequency of dry days for that simulation. For moderate DPE (10-20 mm/day), the 15-km PF is little more than 6% which is greater than the observed PF of 5%. To its turn, the 45-km PF for such DPE is slightly inferior to 6%. For heavy DPE (20-40 mm/day), the 15-km PF and the 45-km PF is respectively of 2.7% and 2.3%, compared to an observed PF of 2.4%. Lastly, the frequency of very heavy DPE (> 40 mm/day) is about 0.5% for the high-resolution simulation, which is closer to the observed PF. On the other hand, the 45-km simulation depicts a frequency about

0.2% inferior than the observed PF for those DPE. The major differences between the two simulations regarding the daily PF distribution are then found at both tips of the distribution (light DPE and very heavy DPE). As a result, the 15-km daily PF distribution is slightly more realistic than the 45-km daily PF distribution.

Similar observations can be made with the spatial frequency histogram displayed in Figure 20b. In effect, the major difference between the two simulations is found at the tail of the distributions. Within the 15-km simulation, the spatial frequency of very heavy DPE (mainly DPE with more than 45 mm) is closer to observations than within the 45-km simulation. In fact, the number of 45-km grid points producing DPE with more than 45 mm is much lower than the number of weather stations registering that type of DPE. In other words, very heavy DPE are sporadic and localised, but they are even more sporadic and localised within the 45-km simulation than what is observed.

On top of showing their major difference in spatial frequency for very heavy DPE, the two simulations also have their greater disagreement concerning the mean PI for such events (Fig. 20c). In fact, within both simulations the mean PI of light to heavy DPE is slightly greater than what is observed. For very heavy DPE though, the 15-km and 45-km PI is respectively of 46.2 mm/day and 45.9 mm/day, which is inferior to the observed intensity of 47.8 mm/day.

Since the light DPE are the most frequent, they are the ones contributing the most to the annual total for observations as well as for model simulations (Fig. 20d). Because of a greater intensity than observed though, the simulated APA accumulated by light DPE is greater than the observed APA of 366 mm. The two simulations also produce more precipitation than observed with moderate DPE due to a greater frequency and intensity. For heavy DPE, the 15-km APA is still about 30 mm superior to the observed APA of 230 mm while the 45-km APA is about 6 mm below observed. Within the simulations E15 and E45, the very heavy DPE respectively contribute to 90 mm/year and 47 mm/year, compared to an observed contribution of 114 mm/year. As a result, the 45-km total APA is of 936 mm while the 15-km total APA is of 1045 mm. The 15-km total APA is than greater than the observed APA of 973

mm while the 45-km total APA is lower. The 45-km total APA may be closer to the observed value, but this comes from a less realistic daily PF and APA distributions (Fig. 20a-d).

4.2.3 Analysis of the water cycle components over the Quebec-Labrador watersheds

Up to now, we have only analyzed the precipitation and other variables for either all the domain of interest or for particular grid points (when compared to observations). We though it would be interesting to see how the 15-km variables look compared to 45-km ones over a smaller area. We analyzed the components of the hydrological cycle (precipitation, liquid and solid precipitation, evapotranspiration, convergence of humidity, runoff) as well as the screen temperature and snow water equivalent over 21 watersheds of the province of Quebec and Labrador. Table 4.3 gives a list of the 21 watersheds, with their abbreviated names, their drainage area, and the number of CRCM4 45-km grid cells. Figure 21 can be consulted for the geographical position of these watersheds.

Both simulations seem to agree about the following aspects. Precipitation (Fig. 22c) is greater in the southwestern part of Quebec and is lower in the north/northeastern part of Quebec (north-south precipitation gradient). The liquid precipitation (Fig. 23c) is also characterized by the same north-south gradient while solid precipitation (Fig. 23d) shows a inversed (south-north) gradient, with higher snowfall rate in the north than in the south. It is also noticeable that most of the precipitation over the province of Quebec falls as rain since the ratio liquid/solid precipitation is about 75 % in the south (RDO watershed) and drops to 62 % in the north (ARN watershed). The north-south precipitation gradient is accompanied by a north-south evapotranspiration gradient (Fig. 22b), convergence of humidity gradient (Fig. 22a) and temperature gradient (Fig. 23a). The snow water equivalent (Fig. 23b) also shows a north-south gradient. Therefore, the higher temperatures in the southern part of Quebec are accompanied by more evapotranspiration and convergence of humidity, which leads to a greater precipitation rate.

The main differences between the two simulations are given in the following. For all the watersheds, the 15-km screen temperature is below the 45-km screen temperature. At 15-km, the total precipitation is greater than at 45-km over all the watersheds. The liquid precipitation follows the same pattern while the solid precipitation does not. Over 10 watersheds out of 21 (mostly located in the north-eastern part of Quebec), the mean solid precipitation is higher at 45-km than it is at 15-km, with the highest difference being in the order of 10 %. This is also visible through the snow water equivalent. Moreover, for 13 watersheds out of 21, the 15-km run reproduces a higher runoff (Fig. 22d) than the 45-km run. According to the study of Music et al. (2009), the CRCM (operational version with horizontal resolution of 45 km) tends to underestimate the observed annual mean runoff. So, the greater value of this variable reproduced by the 15-km run could signify an improvement. Since the maximum of runoff is highly linked with the melting of snow, the snow water equivalent has an important impact on this variable. Indeed, we notice that the watersheds with a higher snow water equivalent at 15 km than at 45 km correspond to the watersheds having greater runoff at 15 km than at 45 km (e.g. ROM). To recapitulate, the 15-km simulation tends to generate more evapotranspiration and convergence of humidity than does the 45-km run, meaning that more humidity is available for precipitation within the 15-km simulation than within the 45-km simulation. Because the 15-km run is slightly cooler than the 45-km run, this humidity condenses more easily and then precipitates more easily as well. This explains why the 15-km precipitation is greater than the 45-km precipitation for all the 21 watersheds.

5 Summary and Conclusion

The inefficacy of most climate models to properly reproduce the intensity and frequency of precipitation is an important problem that needs to be further investigated. This issue is becoming more important as changes in precipitation patterns have already been observed in many regions around the globe (Groisman et al, 2005). In fact, increases in air temperature and specific humidity lead to an enhancement of the hydrological cycle, which should result in a higher frequency of heavy precipitation events and droughts (Trenberth 1999, Trenberth 2003). Using a Regional Climate Model (RCM) to simulate precipitation on a regional scale is now the most efficient and common procedure. With the ongoing progress seen in Computer Science, it is now feasible to produce a high horizontal-resolution simulation over an area of interest at low computer cost. Under the assumption that increasing a RCM's horizontal resolution leads to a better representation of small-scale features, which should improve the simulated precipitation (especially the frequency and intensity), the present study was carried out.

The main objective of this research was to investigate the sensitivity of precipitation to horizontal resolution within the fourth generation of the Canadian Regional Climate Model (CRCM). The study, however, was not limited to the analysis of total precipitation, but was also performed on the components of the hydrological cycle (convergence of humidity, evapotranspiration, liquid and solid precipitation, and runoff) as well as on the surface temperature, snow water equivalent and number of wet days. To accomplish this task, we used two pairs of simulations over two different regions of Canada: western Canada (WEST CAN domain), and eastern Canada (EAST CAN domain). For both domains, we used two 4-year-long simulations nested at their boundary by the reanalysis NCEP NRA2. The first simulation consisted of a run with a horizontal resolution of 15 km while the second simulation was characterised by a horizontal resolution of 45 km. Most of the analysis in this study consisted of a qualitative comparison between the CRCM 15 km simulations and the CRCM 45 km simulations. It also included a comparison between the CRCM-simulated precipitation and the observed precipitation, using hourly precipitation data.

Our research revealed that results were similar for both domains, with only minor differences. For the two domains, the investigation showed that the topography is more realistic within the high resolution simulations (15 km) than within the low resolution simulations (45 km). Nevertheless, because the EAST CAN domain has a much flatter terrain than the WEST CAN domain, increasing horizontal resolution has a weaker effect on the model topography over that area.

Over the WEST CAN domain, topography is the main factor influencing the meteorological variables. In effect, the position of the observed maximum of precipitation, that is west of the Coastal Range (Pacific coast) and west of the Rocky Mountains, were well captured by both simulations (W15 and W45). The more realistic representation of topography found in the 15-km simulation led to an increase in convergence of humidity, especially along the Pacific coast. The analysis also revealed that the 15-km simulation produces globally more evapotranspiration than the 45-km simulation. As a consequence, the 15-km precipitation is overall superior to the 45-km precipitation, especially along the Pacific coast. Moreover, both simulations agreed that the main source of humidity used to generate most of the precipitation is convergence. Furthermore, results showed that the maximum of convergence occurs in winter for both simulations, which is also the wettest season observed. Results also established that evapotranspiration is maximal during summer. The higher-resolved topography present in the 15-km simulation also led to a greater number of wet days for the 15-km run than for the 45-km over the Pacific Ocean as well as west of the mountains. On the lee side of the mountains and hills, the number of wet days is lower for the 15-km run than for the 45-km run. We also found that over the WEST CAN domain, most of the precipitation falls in its liquid form and that the 15-km liquid precipitation is greater than that of the 45-km. For solid precipitation, our analysis showed that it is larger for the simulation W15 than for the simulation W45 over the mountains but not over the prairies. In addition, the finer horizontal resolution in the 15-km simulation allows capturing some of the permanent snow present at the top of the highest mountains. The snow water equivalent is then greater at 15 km than at 45 km for all year around including summer, where the 15-km simulation shows a non-zero snow water equivalent when all the snow has melted in the 45-km simulation. Resulting from a globally inferior solid precipitation and a greater

evapotranspiration, the 15-km simulation generates globally less runoff than the 45-km simulation.

For the EAST CAN domain, the analysis revealed the 15-km simulation (E15) also produces more precipitation than the 45-km simulation (E45). The previous result can be attributed to a greater 15-km convergence of humidity mostly during fall and a greater 15-km evapotranspiration mostly during summer, which are the two wettest season of the year over the EAST CAN domain. Our analysis also showed that summer and fall have more days with precipitation, with the number of wet days being on average superior for the 15-km simulation than for the 45-km simulation. In other words, precipitation occurs more often in the high resolution run than in the low resolution run. Results also divulged that most of the precipitation falls in its liquid form and that for both liquid and solid precipitation, the 15-km simulation produces larger values than the 45-km simulation. Because of having a slightly greater solid precipitation, the 15-km simulation also depicted a greater snow water equivalent than the 45-km simulation, especially over mountains and the north-eastern portion of the domain. Directly linked with the melting of snow and the amount of precipitation, the total runoff was found to be superior for the simulation E15 than for the simulation E45, especially from May to December. This result differs from what we found for the WEST CAN domain. Over the EAST CAN domain, both the solid precipitation and the snow water equivalent are superior for the 15-km simulation than for the 45-km simulation. Therefore, the melting of snow makes the 15-km runoff superior to the 15-km runoff during spring. During the rest of the year, the runoff remains greater for the 15-km simulation than for the 45-km simulation because the 15-km precipitation is superior to the 45-km precipitation.

The further analysis of the water cycle components over the Quebec and Labrador watersheds revealed that the 15-km run is slightly cooler than the 45-km run over all the watersheds. Moreover, with a greater convergence of humidity and evapotranspiration, the 15-km simulation produces more precipitation than the 45-km simulation for all 21 watersheds. The analysis also showed that for 13 watersheds out of 21 the 15-km run produces a higher runoff than the 45-km run. This result could represent an improvement

because the 45-km CRCM (operational version with horizontal resolution of 45 km) tends to underestimate the observed annual mean runoff (Music et al. 2009).

The comparison between simulated and observed precipitation revealed that for both domains, the 15-km and 45-km simulations were able to reproduce the observed annual cycle of precipitation. However, results showed that the simulated monthly precipitation is systematically superior to the observed monthly precipitation, except for the simulation E45. Moreover, the annual cycle revealed that the 15-km monthly precipitation is generally greater than the 45-km monthly precipitation, which is consistent with what we found during the water cycle components analysis. A frequency and intensity analysis made with an hourly accumulation interval divulged that for both domains the model (15-km and 45-km simulations) produces a higher frequency of light Hourly Precipitation Events (HPE; 0.2-3 mm/h) than observed. In fact, the simulated frequency of such events is about twice the observed frequency. Therefore, the Annual Precipitation Amount (APA) produced by these events is about 600 mm and 300 mm greater than observations for the WEST CAN domain simulations and for the EAST CAN domain simulations, respectively. On the other hand, the analysis divulged that contrarily to the simulation W45, the simulation W15 is able to reproduce light (0.2-3 mm/h) to very heavy (>10 mm/h) HPE. In fact, the simulation W45 produces zero heavy (6-10 mm/h) and very heavy HPE. Similar results were found for the EAST CAN domain, where the 45-km PF fell rapidly below the observed PF for events greater than 3 mm/h (moderate to very heavy HPE). Thus, the 15-km hourly Precipitation Frequency (PF) distribution was found to be more realistic than the 45-km one for both domains. The hourly Precipitation Intensity (PI) distribution was also more realistic when obtained with the 15-km simulations than with the 45-km simulations. Because the 45-km simulations (W45 and E45) generate much less moderate to very heavy HPE, it compensates for the excess in precipitation produced by light HPE thereby resulting in a total APA that is slightly closer to observations. For the EAST CAN domain, the 45-km total APA is even slightly below the observed total APA. Despite the more realistic hourly PF and PI distributions found for the 15-km simulations (W15 and E15), the model-observed precipitation bias is greater for the 15-km simulations than for the 45-km simulations because there is no such compensation within the high resolution simulations.

In order to determine if similar results could be found with a greater accumulation period, we also analysed the PF and PI of simulated and observed precipitation with a daily accumulation period. The analysis revealed that the differences between the two simulations were more subtle than when using an hourly accumulation interval. Except for the simulation E45, the excess in precipitation (compared to observations) found in all simulations (W15, W45 and E15) was evenly distributed through the intensity spectrum (from 0.2 to 48 mm/day). As a result, for both domains the 15-km and 45-km simulations seemed to equally be able to reproduce the observed daily PF and PI distributions. This result highlighted the importance of the accumulation period. Using a daily accumulation interval smoothes the short bursts of convective precipitation through time averaging. Moreover, a strong PE is usually not sustained for an entire day (Gutowski Jr. et al., 2003). Therefore, working with a 24-h accumulation period is not as efficient as an hourly accumulation period in understanding which events the model is able to reproduce and what the contribution (in precipitation amount) of each type of events is.

To conclude, we found that the 15-km precipitation is greater than the 45-km precipitation for both domains and that the simulated precipitation tends to be greater than the observed precipitation (true for all simulations but the simulation E45 for the EAST CAN domain). It is important to keep in mind that when comparing simulated precipitation with observed precipitation, no adjustments were made concerning the precipitation gauge under catch. A deeper analysis should be made to see how much the under catch could explain some of the model-observation precipitation bias seen in this study. Moreover, our research was mainly limited to a qualitative comparison between the high and low CRCM-simulated variables and did not include a comparison with gridded observations. Therefore, we recommend that such a comparison be made. When doing so, the gridded observation set should have a horizontal resolution as close as possible to 15 km, in order to verify if the 15-km simulations can capture more small-scale precipitation patterns than the 45-km simulations.

SOMMAIRE ET CONCLUSION

L'inefficacité de la plupart des modèles climatiques à reproduire adéquatement l'intensité et la fréquence de la précipitation est un problème important qui doit être analysé davantage. Ce sujet est d'autant plus important puisque des modifications au comportement de la précipitation ont déjà été observées dans plusieurs régions du monde (Groisman et al, 2005). En fait, l'augmentation de la température de l'air et de l'humidité spécifique amplifie le cycle hydrologique, ce qui devrait faire augmenter la fréquence des événements de précipitation forte et les sécheresses (Trenberth 1999, Trenberth 2003). L'utilisation d'un Modèle Régional du Climat (MRC) pour simuler la précipitation à l'échelle régional est actuellement la méthode la plus efficace et la plus utilisée. Avec les progrès constants en informatique, il est maintenant possible de produire une simulation à haute résolution horizontale à un faible coût informatique. En supposant que l'augmentation de la résolution horizontale d'un MRC entraîne une meilleure représentation des processus de fines échelles, ce qui devrait améliorer la précipitation simulée (particulièrement l'intensité et la fréquence), la présente étude a été menée.

L'objectif principal de cette étude était de déterminer quelle est la sensibilité de la précipitation à la résolution horizontale dans la quatrième génération du Modèle Régional Canadien du Climat (MRCC). Toutefois, notre étude ne s'est pas limitée à l'analyse de la précipitation totale, mais a aussi été réalisé pour les composantes du cycle hydrologique (convergence d'humidité, évapotranspiration, précipitation liquide et solide, et ruissellement) de même que pour la température de surface, l'équivalent en eau de la neige et le nombre de jour de précipitation. Pour ce faire, nous avons utilisé deux paires de simulations au-dessus de deux régions du Canada : l'ouest du Canada (domaine WEST CAN), et l'est du Canada (domaine EAST CAN). Pour chacun de ces domaines, nous avons utilisé deux simulations d'une durée de quatre ans et pilotées à leurs frontières par les réanalyses NCEP NRA2. La première simulation était caractérisée par une résolution horizontale de 15 km, tandis que la seconde simulation avait une résolution horizontale de 45 km. La plupart de l'analyse réalisée

au sein de cette étude consistait en une comparaison qualitative entre les simulations à 15 km de résolution et celles à 45 km de résolution. Une comparaison entre la précipitation simulée et observée a également été effectuée, en utilisant des données de précipitation horaire.

Notre recherche a révélée que les résultats étaient similaires pour les deux domaines, avec seulement quelques différences mineurs. Pour les deux domaines, l'étude a démontré que la topographie est plus réaliste au sein des simulations à haute résolution (15 km) que dans celles à basse résolution (45 km). Néanmoins, étant donné que le domaine EAST CAN a un terrain beaucoup moins accidenté que le domaine WEST CAN, l'augmentation de la résolution horizontale a un effet moins remarquable sur la topographie au-dessus de cette région.

Pour le domaine WEST CAN, notre recherche a permis de révéler que la topographie est le principal élément influençant les variables météorologiques. En effet, la position du maximum de précipitation observé, qui est à l'ouest de la chaîne côtière (le long de la côte) et à l'ouest des Rocheuses, est bien reproduit par les deux simulations (W15 et W45). La représentation plus réaliste de la topographie retrouvée dans la simulation à 15 km mène à une augmentation de la convergence d'humidité, particulièrement le long de la côte du Pacifique. Notre analyse a aussi révélée que la simulation à 15 km produit davantage d'évapotranspiration que la simulation à 45 km. Par conséquent, la simulation W15 génère globalement plus de précipitation que la simulation W45, particulièrement le long de la côte Pacifique. De plus, les deux simulations étaient en accord avec le fait que la principale source d'humidité utilisée pour générer la précipitation est la convergence. Les résultats démontrent également que pour les deux simulations, le maximum de convergence d'humidité se produit l'hiver, soit la saison enregistrant le plus de précipitation durant l'année. Pour ce qui est de l'évapotranspiration, les résultats ont établi qu'elle est maximale pendant l'été. La topographie mieux résolue au sein de la simulation à 15 km mène à un nombre de jours de précipitation par année supérieur que dans la simulation à 45 km au-dessus de l'océan Pacifique et du côté ascendant des montagnes. Toutefois, du côté descendant des montagnes et collines, le nombre de jours de précipitation par année est inférieur pour la simulation à 15 km que pour celle à 45 km. Nous avons aussi trouvé que pour le domaine WEST CAN, la

majorité de la précipitation tombe sous forme liquide, avec la précipitation liquide étant supérieure dans la simulation à 15 km que dans celle à 45 km. Pour ce qui est de la précipitation sous forme solide, la simulation W15 montre de valeurs plus élevées que la simulation W45 au-dessus des montagnes, mais pas au-dessus des prairies. Également, l'augmentation de la résolution permet à la simulation à 15 km de produire de la neige éternelle au sommet des plus hautes montagnes du domaine. L'équivalent en eau de la neige est alors supérieur dans la simulation W15 pendant toute l'année, incluant l'été, où la simulation à 15 km de résolution a un l'équivalent en eau de la neige supérieur à zéro tandis que toute la neige est fondue dans la simulation à 45 km de résolution. Résultant d'une précipitation solide globalement inférieure et d'une plus grande évapotranspiration, la simulation à 15 km produit davantage de ruissellement que la simulation 45 km.

Pour le domaine EAST CAN, l'analyse a révélé que la simulation à 15 km (E15) produit également davantage de précipitation que la simulation à 45 km (E45). Ceci peut être attribué à une convergence d'humidité plus grande à 15 km qu'à 45 km pendant l'automne et à une évapotranspiration supérieure à 15 km pendant l'été. Par ailleurs, l'été et l'automne sont les deux saisons recevant le plus de précipitation pour le domaine EAST CAN. Notre analyse a aussi démontré que ces deux saisons sont celles enregistrant le plus grand nombre de jours de précipitation, et ce nombre est supérieur au sein de la simulation à 15 km qu'au sein de la simulation à 45 km. Bref, la précipitation est plus fréquente dans la simulation à haute résolution que dans celle à basse résolution. Les résultats illustrent aussi que la majorité de la précipitation tombe sous forme liquide, et qu'autant pour la précipitation liquide que solide, les valeurs sont plus élevées dans la simulation à 15 km que dans celle à 45 km. Puisque la précipitation solide est légèrement plus grande dans la simulation E15 que la simulation E45, l'équivalent en eau est également supérieur, particulièrement au-dessus des montagnes et au-dessus de la partie nord-est du domaine. Directement lié avec la fonte de la neige et la quantité de précipitation, le ruissèlement total est supérieur pour la simulation à 15 km que pour la simulation à 45 km, particulièrement entre mai et décembre. Ce dernier constat diffère de ce que nous avons trouvé pour le domaine WEST CAN. Dans le domaine EAST CAN, la précipitation solide et l'équivalent en eau de la neige sont tous les deux supérieurs à 15 km qu'à 45 km. Par conséquent, le ruissèlement de surface est plus grand dans la

simulation à 15 km que dans la simulation à 45 km au printemps. Durant le reste de l'année, le ruissèlement demeure supérieur à 15 km qu'à 45 km parce que la précipitation est aussi supérieure à 15 km qu'à 45 km.

L'analyse des composantes du cycle hydrologique pour les bassins versants de la province de Québec et du Labrador a révélée que la simulation E15 est légèrement plus froide que la simulation E45, et ce pour tous les bassins versants. De plus, produisant davantage de convergence d'humidité et d'évapotranspiration, la simulation à 15 km de résolution génère également davantage de précipitation que la simulation à 45 km pour les 21 bassins versants. Notre analyse illustre aussi que pour 13 bassins sur 21, la simulation à 15 km produit un ruissèlement supérieur à celui produit par la simulation à 45 km. Ce résultat pourrait représenter une amélioration, puisque le MRCC à 45 km (version opérationnelle avec une résolution de 45 km) sous-estime généralement le ruissèlement annuel moyen observé (Music et al. 2009).

La comparaison entre la précipitation simulée par le MRCC et la précipitation observée a révélé que pour les deux domaines, les simulations à 15 km et 45 km étaient capables de reproduire le cycle annuel observé. Toutefois, les résultats démontrent que la précipitation mensuelle simulée est systématiquement supérieure à la précipitation mensuelle observée, excepté pour la simulation E45. De plus, le cycle annuel a révélé que la précipitation mensuelle des simulations à 15 km est généralement supérieure celle des simulations à 45 km, ce qui est en accord avec les résultats trouvés lors de l'analyse des composantes du cycle hydrologique. Une analyse de la fréquence et intensité de la précipitation faite à partir d'une période d'accumulation d'une heure a révélé que pour les deux domaines, le modèle (15 km et 45 km) produit une plus grande fréquence d'événements horaires de faibles intensités (0,2-3 mm/h) que ce qui est observé. En fait, la fréquence simulée de ce type d'événements est environ deux fois plus grande que la fréquence observée. Par conséquent, la quantité de précipitation accumulée annuellement par les événements horaires de faible intensité est environ 600 mm et 300 mm plus grande que la quantité observée pour les simulations du domaine WEST CAN et du domaine EAST CAN, respectivement. D'un autre côté, notre analyse a démontré que contrairement à la simulation W45, la simulation W15 est capable de

reproduire des événements horaires d'intensités faibles (0,2-3 mm/h) à très fortes (> 10 mm/h). En fait, la simulation W45 ne produit aucun événement horaire d'intensité forte et très forte. Des résultats similaires ont été trouvés pour le domaine EAST CAN, où la fréquence de la précipitation pour la simulation E45 tombait rapidement sous la fréquence observée pour les événements d'intensités supérieures à 3 mm/h (intensité modérée à très forte). Donc, la distribution horaire de la fréquence de la précipitation était plus réaliste lorsqu'elle était obtenue à partir des simulations à hautes résolutions (W15 et E15) qu'avec les simulations à basses résolutions (W45 et E45). La distribution horaire de l'intensité de la précipitation était également plus réaliste lorsqu'elle était obtenue à partir des simulations à 15 km. Puisque les simulations à 45 km (W45 et E45) génèrent beaucoup moins d'événements d'intensités modérées à fortes, ceci compense pour l'excès en précipitation généré par les événements de faibles intensités, ce qui résulte en une précipitation annuelle totale qui plus près de celle observée. Pour le domaine EAST CAN, la précipitation annuelle totale produit par la simulation à 45 km est même légèrement inférieure à celle observée. Malgré que les distributions horaires de fréquence et d'intensité soient plus réalistes pour les simulations à 15 km (W15 et E15), le biais de précipitation model-observation est plus grand pour les simulations à 15 km que pour celles à 45 km puisque ce type de compensation n'existe pas au sein des simulations à hautes résolutions.

Afin de déterminer si de résultats similaires pouvaient être retrouvés en utilisant une période d'accumulation plus grande, nous avons également analysé la fréquence et l'intensité de la précipitation simulée et observée à partir d'une période d'accumulation de 24 heures. Notre analyse a démontré que les différences entre les deux simulations étaient beaucoup plus subtiles que lorsque nous utilisions une période d'accumulation d'une heure. À l'exception de la simulation E45, l'excès de précipitation (comparativement aux observations) retrouvé dans toutes les simulations (W15, W45 et E15) est également distribué à travers le spectre des intensités (0,2 à 48 mm/jour). Par conséquent, pour les deux domaines, les simulations à 15 km et à 45 km de résolution semblaient être également capables de reproduire les distributions journalières observées de la fréquence et de l'intensité. Ce résultat a permis de mettre en évidence l'importante de la période d'accumulation. L'utilisation d'une période d'accumulation de 24 heures fait que les événements convectifs intenses sont atténués par la

moyenne temporelle. De plus, un événement très intense ne durera généralement pas toute la journée (Gutowski Jr. et al., 2003). Donc, déterminer quel(s) type(s) d'événement(s) le modèle est capable de reproduire et quel est la contribution (en termes de quantité de précipitation) de chacun de ces événements n'est pas aussi efficace lorsqu'une période d'accumulation de 24 heures est utilisée à la place qu'une période d'accumulation d'une heure.

En conclusion, pour les deux domaines, la précipitation est supérieure au sein des simulations à 15 km de résolution que dans celle à 45 km de résolution. De plus, la précipitation simulée par le MRCC4 est généralement supérieure à la précipitation observée (vrai pour toutes les simulations, sauf la simulation E45 du domaine EAST CAN). Il est important de se rappeler que lorsque nous avons comparé la précipitation simulée avec la précipitation observée, aucun ajustement n'a été fait concernant le sous-captage des appareils mesurant la précipitation. Une étude plus approfondie devrait être menée afin de déterminer comment et si le sous-captage des appareils pourrait expliquer une partie du biais model-observations (pour la précipitation) retrouvé dans cette étude. De plus, notre recherche était principalement limitée à une comparaison qualitative entre les variables simulées par les simulations à 15 km versus celles simulées par les simulations à 45 km et n'incluait pas de comparaison avec des observations sur grille. Donc, nous recommandons qu'une telle comparaison soit faite. En faisant cette comparaison, la résolution horizontale des observations sur grille devrait être aussi près que possible de 15 km, pour ainsi permettre de vérifier si le champ de précipitation de la simulation à 15 km reproduit davantage de processus de fine échelle que le champ de précipitation de la simulation à 45 km.

TABLEAUX

Table 3.1 Main characteristics of the simulations used in this study

Domain	Simulation name	Horizontal resolution (km)	Grid dimension* (NI x NJ)	Time step (minutes)
WEST CAN	W15	15	120 x 120	5
	W45	45	40 x 40	15
EAST CAN	E15	15	165 x 165	5
	E45	45	55 x 55	15

* : The grid dimension does not include the 10-grid point sponge zone

Table 4.1 Mean annual precipitation amount (mm/year) and mean number of wet days (days/year) observed at Victoria Int'l Airport and North Vancouver Sonora Dr, and simulated at the closest grid points to those weather stations

	Mean annual precipitation amount (mm/year)		
Name of weather station	Observed at the weather station	Simulated at the closest grid point to the weather station	
		W15	W45
Victoria Int'l A	783	1264	1409
North Vancouver Sonora Dr	1975	2865	2516
PCP*(Vancouver)/PCP(Victoria)	2,5	2,3	1,8
	Mean number of wet days (days/year)		
Name of weather station	Observed at the weather station	Simulated at the closest grid point to the weather station	
		W15	W45
Victoria Int'l A	138	166	198
North Vancouver Sonora Dr	163	175	212

*PCP : Precipitation

Table 4.2 Altitude (m) at the weather stations Victoria Int'l Airport and North Vancouver Sonora Dr as well as the altitude (m) at the closest grid points and at the most representative grid points to those stations

Name of weather station	weather station	closest GP* to the weather station		most representative GP* to the weather station	
	observed	W15	W45	W15	W45
Victoria Int'l A	19	23	88	23	88
North Vancouver Sonora Dr	5	395	526	94	119

*GP : Grid point

Table 4.3 List of the 21 watersheds with their respective abbreviated name, drainage area and number of 45-km CRCM grid points

Watershed Name	Abbreviation	Drainage area km^2	Number of CRCM 45-km grid points*
Rivière Arnaud	ARN	26900	14
Rivière à la Baleine	BAL	29000	17
Rivière Bell	BEL	22200	15
Bersimis-Outardes-Manie	BOM	87000	47
Réservoir Caniapiscau	CAN	37870	23
Réservoir Churchill Falls	CHU	69300	34
Rivière aux Feuilles	FEU	41700	22
Rivière Georges	GEO	24200	11
Grande rivière de la Baleine	GRB	36300	18
La Grande Rivière	LGR	177000	91
Réservoir Manic5	MAN	29240	17
Rivière aux Mélèzes	MEL	42700	22
Rivière Moisie	MOI	19000	12
Rivière Natashquan	NAT	15600	9
Rivière Caniapiscau (Pyrite)	PYR	48500	24
Rivière des Outaouais	RDO	143000	80
Rivière Romaine	ROM	13000	9
Rivière Rupert	RUP	40900	22
Lac Saint-Jean	SAG	73000	43
Rivière Saint-Maurice	STM	47200	28
Rivière Waswapini	WAS	31900	16

* : The number of CRCM 15-km grid points is simply the number of CRCM 45-km grid points multiplied by a factor of 9.

FIGURES

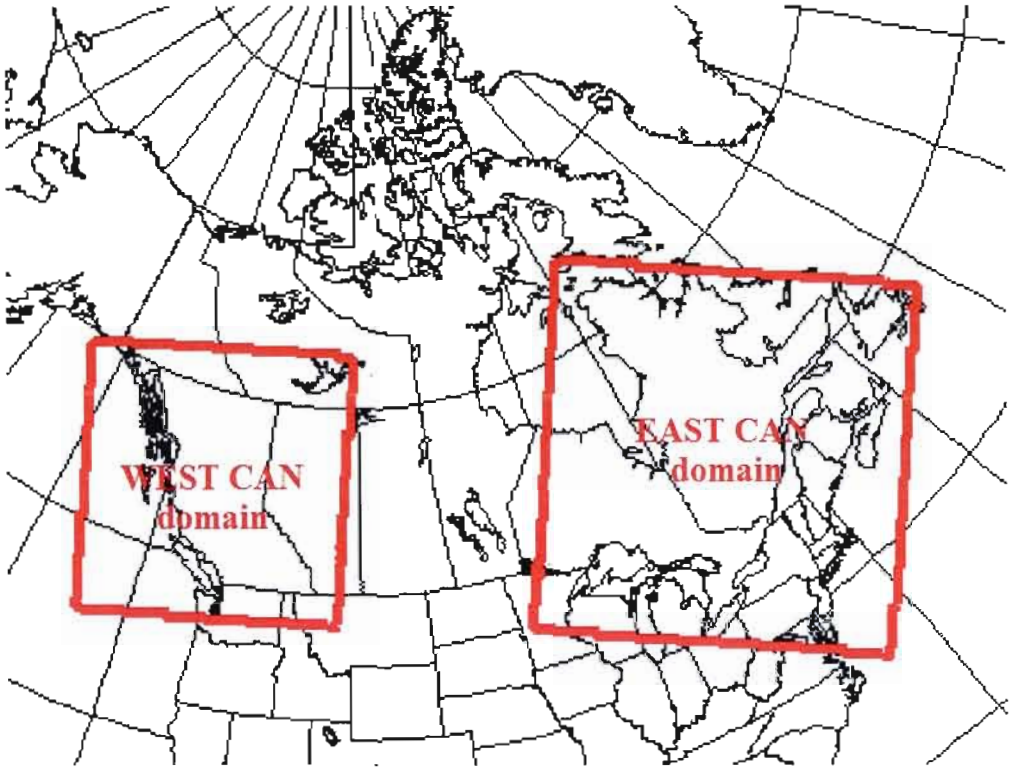

Figure 1 Geographical position of the two CRCM4 simulation domains (WEST CAN and EAST CAN) used in this study.

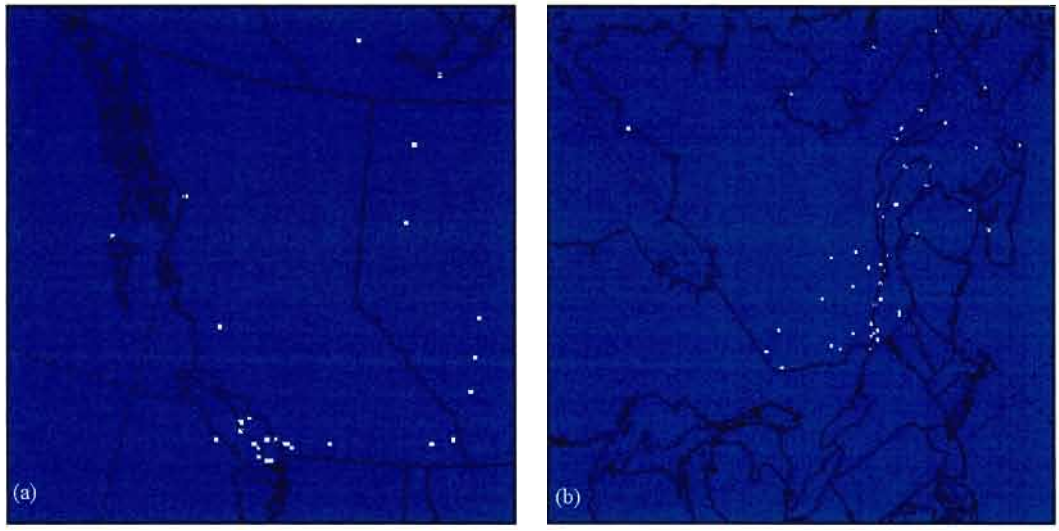

Figure 2 Position of the weather stations of the Environment Canada's hourly-precipitation network on the 15-km grid (in white) over (a) the WEST CAN domain and (b) the EAST CAN domain. Only stations kept for analysis are shown. A total number of 27 stations is used over the WEST CAN domain (a) and a total of 45 stations is used over the EAST CAN domain (b).

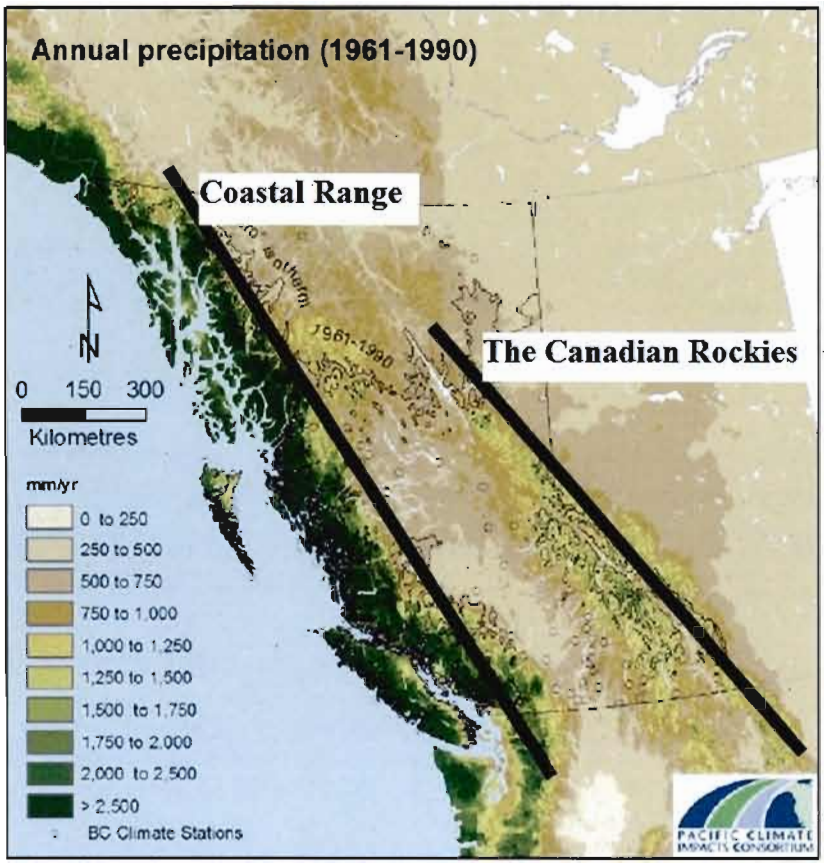

Figure 3 Mean annual precipitation amount observed (1961-1990) over the WEST CAN domain with the position and name of the main topographic barriers (after the Pacific Climate Impacts Consortium, PCIC).

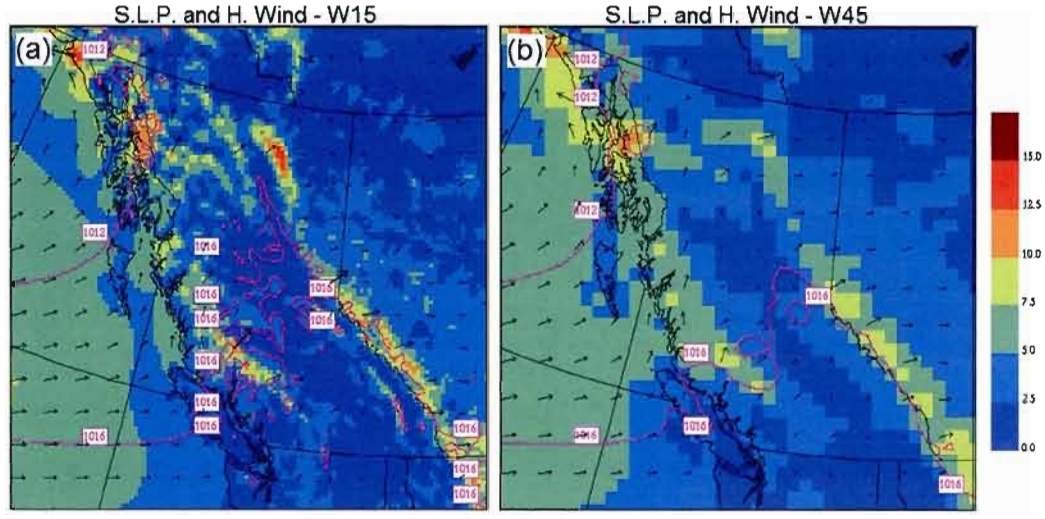

Figure 4 4-year annual mean sea level pressure (magenta contours; hPa), horizontal wind speed (background filed contours; km/h) and horizontal wind direction (black arrows) for the simulations W15 (a) and W45 (b).

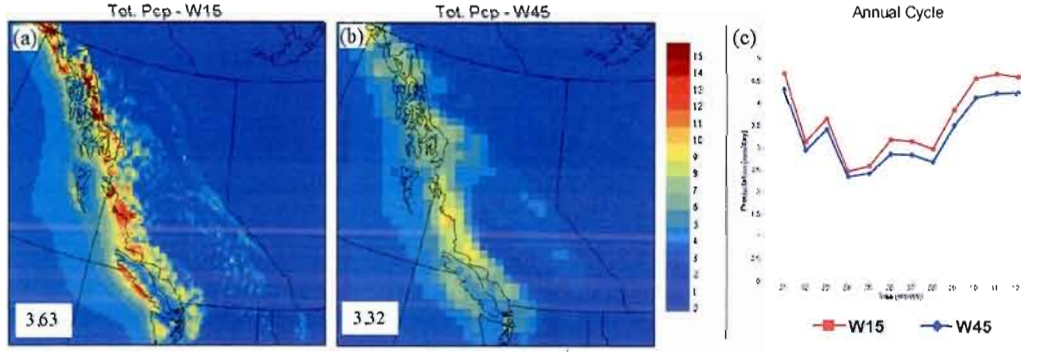

Figure 5 4-year annual mean total precipitation rate (mm/day) for the simulations W15 (a) and W45 (b). Panel (c) shows the domain-averaged mean annual cycle of total precipitation. On the bottom left corner of panels (a) and (b) is given the domain average of the total precipitation rate (mm/day).

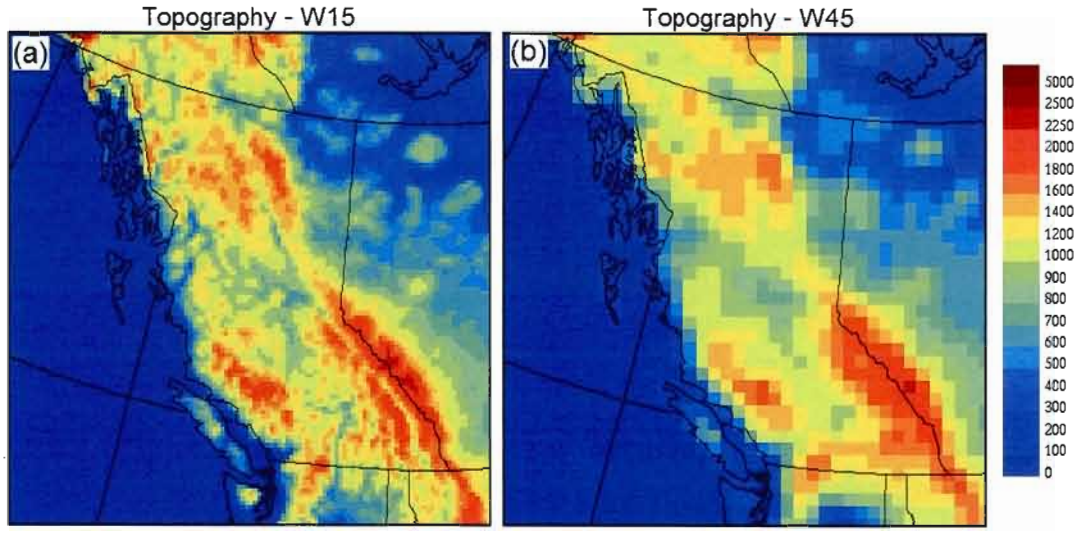

Figure 6 Topography (m) of the simulations W15 (a) and W45 (b).

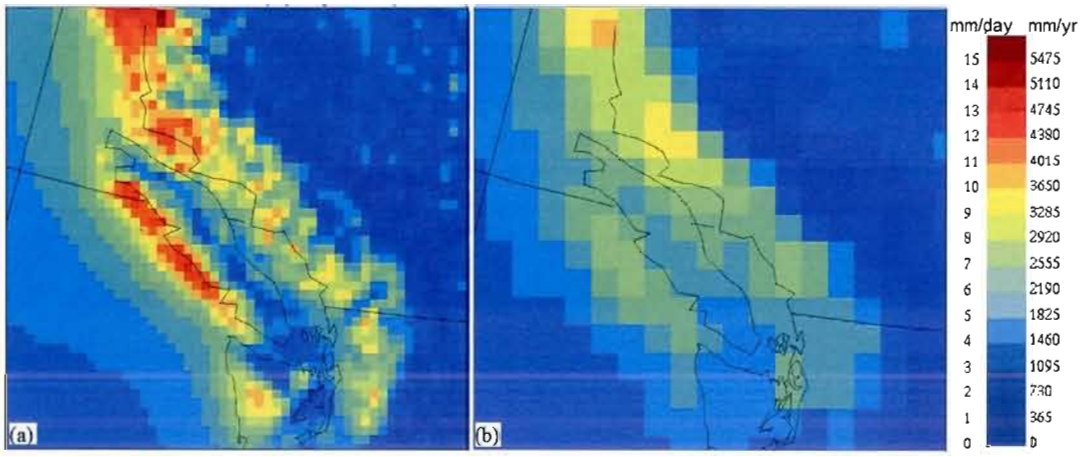

Figure 7 4-year annual mean total precipitation rate (mm/day or mm/year) for the simulations W15 (a) and W45 (b) zoom over a portion of the WEST CAN domain surrounding the Vancouver and Victoria area.

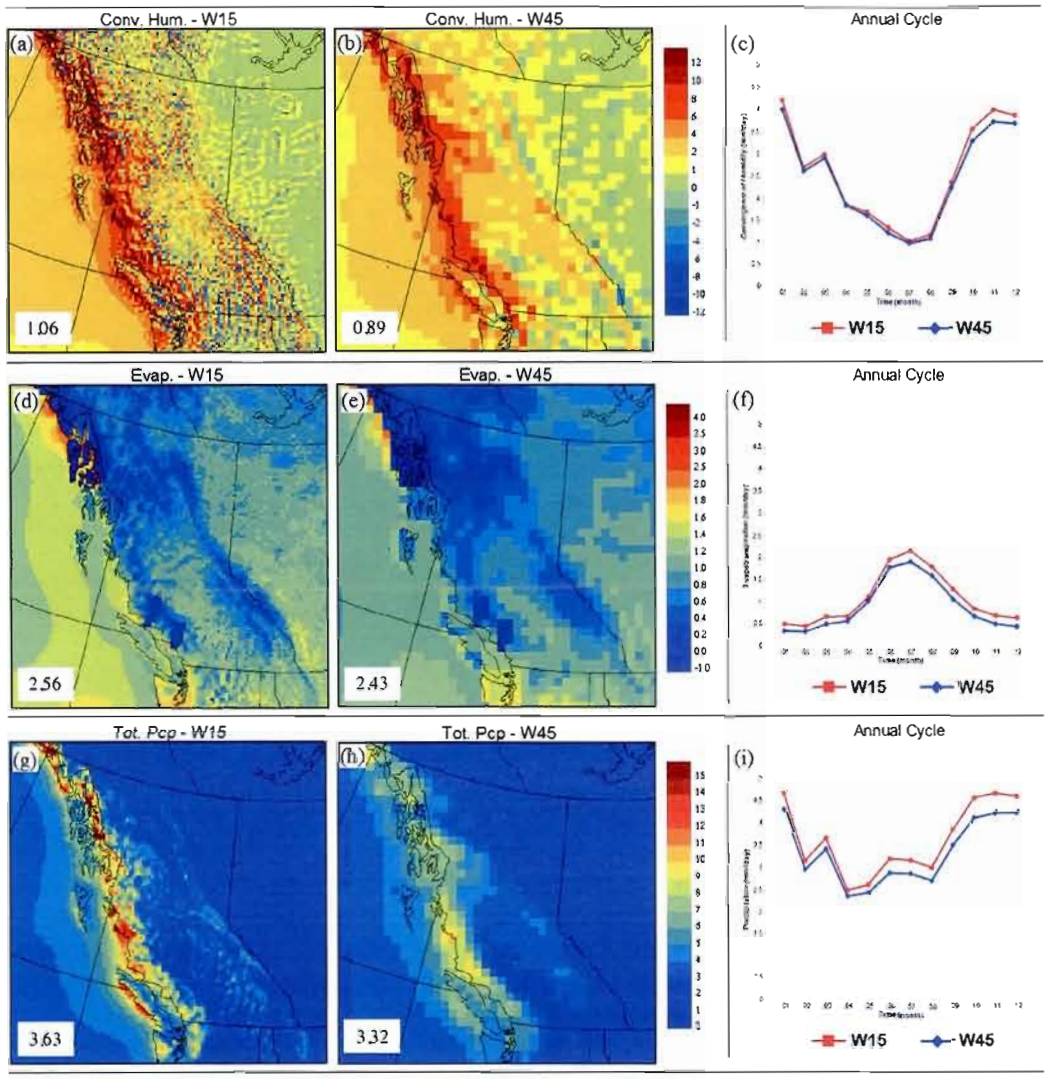

Figure 8 Top: 4-year annual mean convergence of humidity (mm/day) for the simulations W15 (a) and W45 (b). Panel (c) depicts the domain-averaged mean annual cycle of convergence of humidity. Middle: 4-year annual mean evapotranspiration (mm/day) for the simulations W15 (d) and W45 (e). Panel (f) presents the domain-averaged mean annual cycle of evapotranspiration. Bottom: 4-year annual mean total precipitation rate (mm/day) for the simulations W15 (g) and W45 (h). Panel (i) shows the domain-averaged mean annual cycle of total precipitation. On the bottom left corner of panels (a), (b), (d), (e), (g) and (h) is given the domain average of the respective variables.

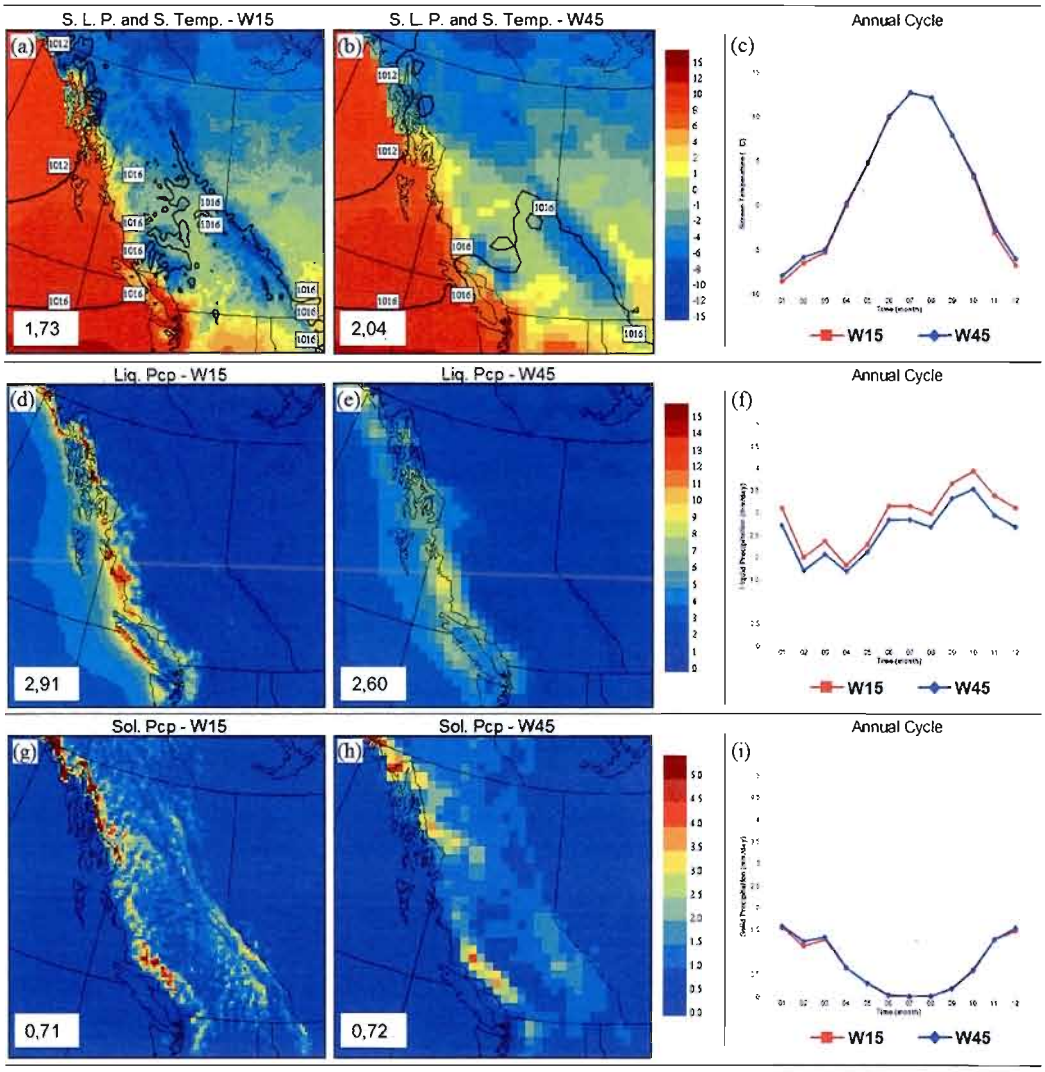

Figure 9 Top: 4-year annual mean sea level pressure (black contours; hPa) and screen temperature (°C) for the simulations W15 (a) and W45 (b). Panel (c) shows the domain-averaged mean annual cycle of screen temperature. Middle: 4-year annual mean liquid precipitation rate (mm/day) for the simulations W15 (d) and W45 (e). Panel (f) presents the domain-averaged mean annual cycle of liquid precipitation. Bottom: 4-year annual mean solid precipitation rate (mm/day) for the simulations W15 (g) and W45 (h). Panel (i) depicts the domain-averaged mean annual cycle of solid precipitation. On the bottom left corner of panels (a), (b), (d), (e), (g) and (h) is given the domain average of the respective variables.

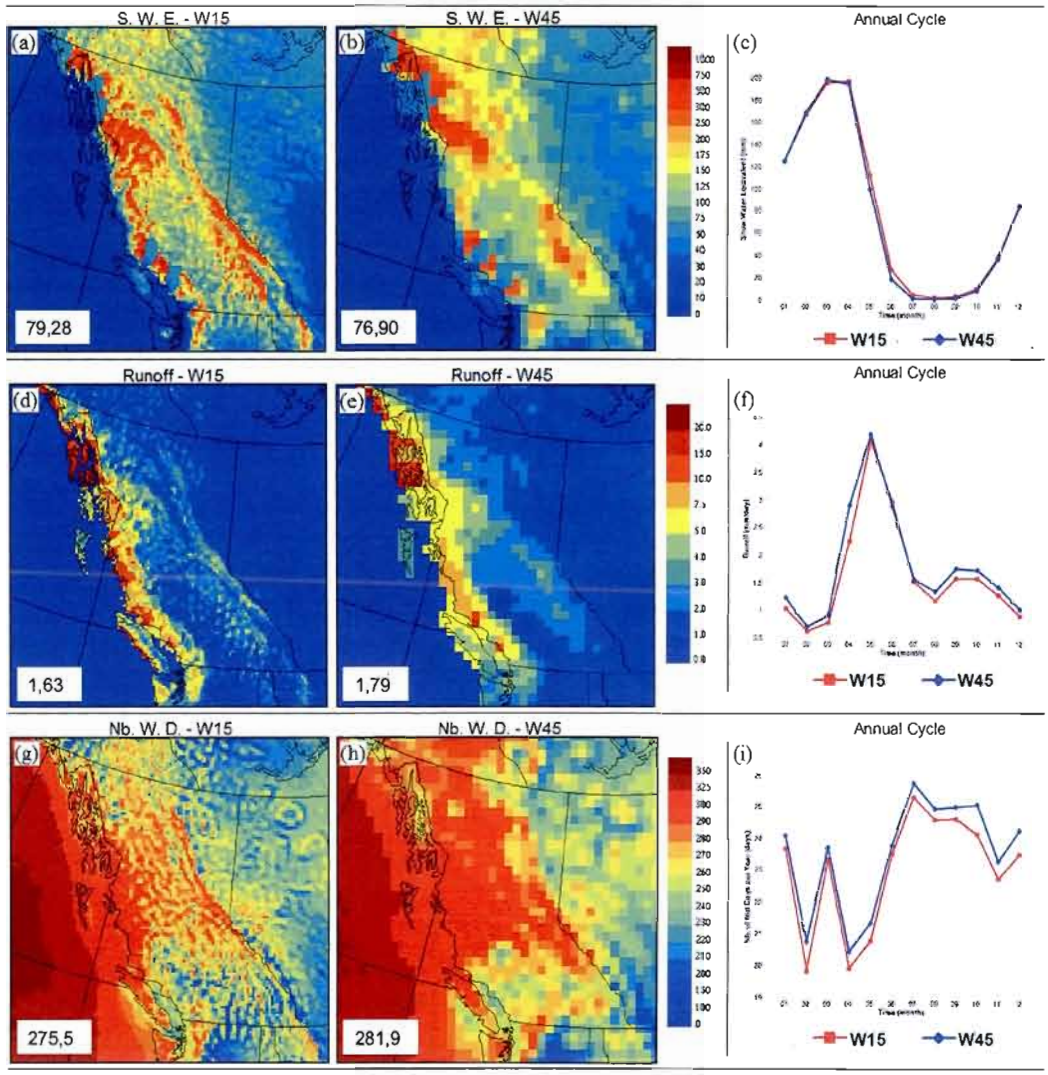

Figure 10 Top: 4-year annual mean snow water equivalent (mm) for the simulations W15 (a) and W45 (b). Panel (c) presents the domain-averaged mean annual cycle of snow water equivalent. Middle: 4-year annual mean runoff (mm/day) for the simulations W15 (d) and W45 (e). Panel (f) shows the domain-averaged mean annual cycle of runoff. Bottom: 4-year mean number of wet days (days/year) for the simulations W15 (g) and W45 (h). Panel (i) presents the domain-averaged mean annual cycle of the number of wet days. On the bottom left corner of panels (a), (b), (d), (e), (g) and (h) is given the domain average of the respective variables.

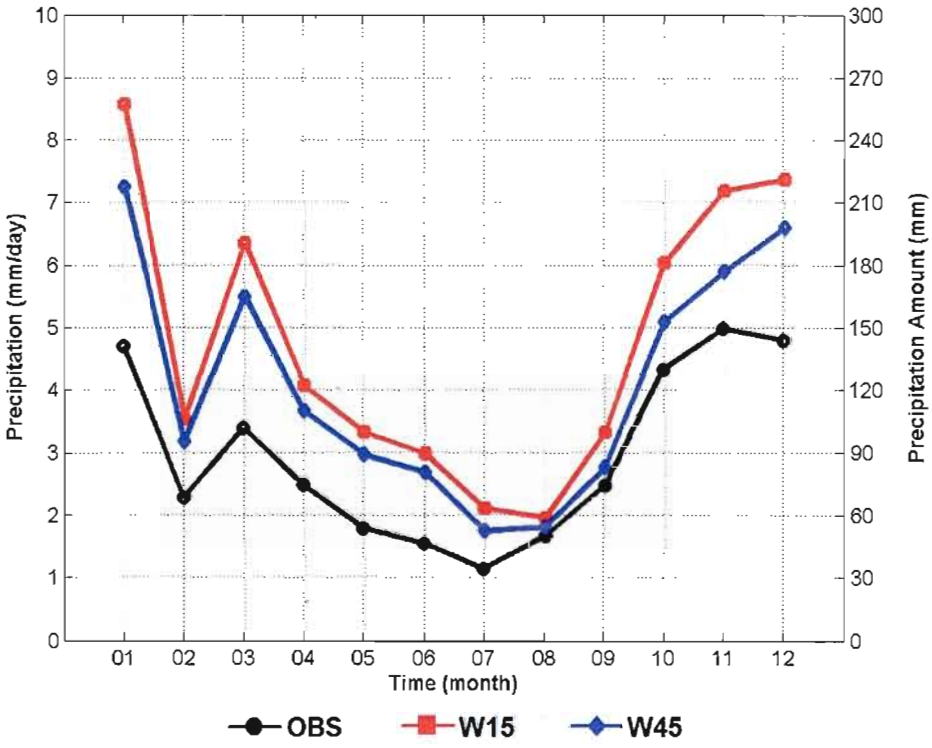

Figure 11 Mean annual cycle of precipitation (mm/day and mm) for model simulations (W15 and W45) and observations. The curves represent the mean annual cycle of all the 27 stations (for observations) or grid points (for model simulations) used in this study (see section *3.3*).

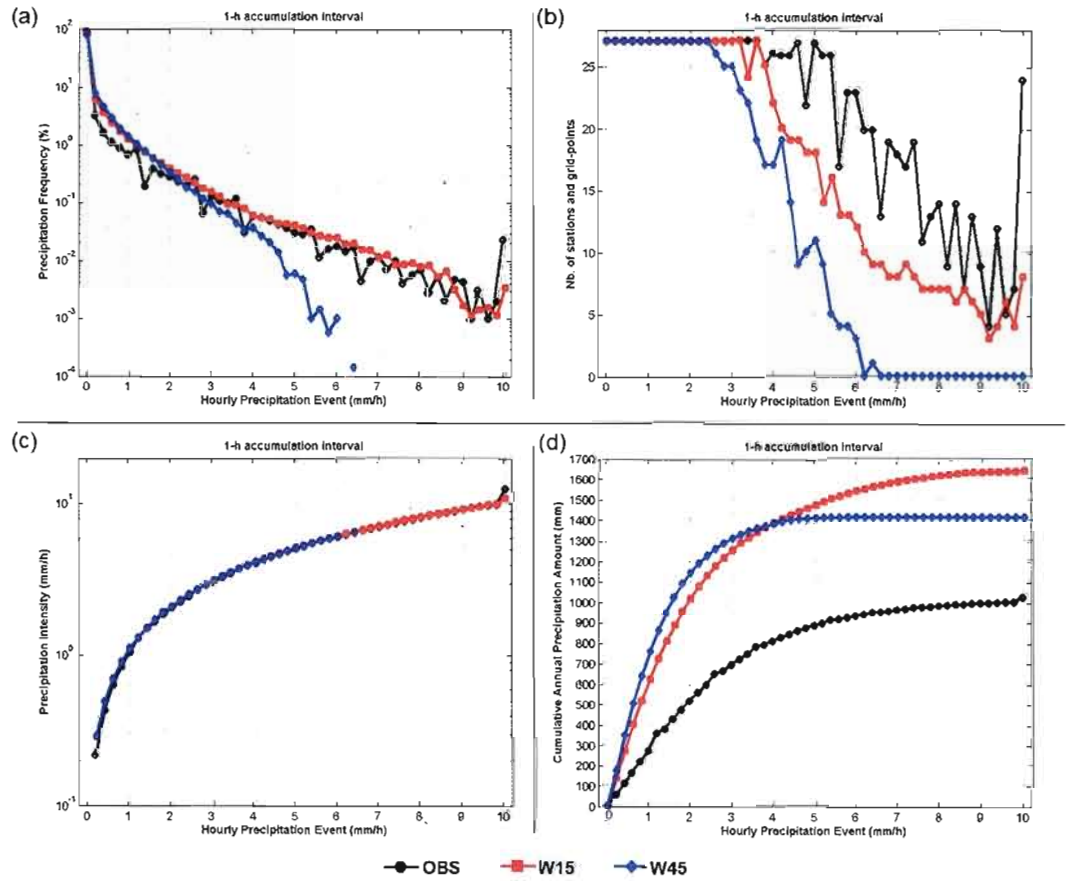

Figure 12 Observed and simulated (W15 and W45) distributions obtained with a 1-h accumulation interval. (a) 4-year mean precipitation frequency (%), (b) 4-year mean number of weather stations (for observations) and grid points (for model), (c) 4-year mean precipitation intensity (mm/h), and (d) 4-year mean cumulative annual precipitation amount (mm). The x-axis represents the Hourly Precipitation Event (HPE) in units of mm/h, with the number on the axis being the threshold of a HPE class. The width of each HPE class is 0.2 mm/h. On each panel, the curves represent the mean distributions of all the 27 weather stations (for observations) or grid points (for model simulations) used in this study (see section *3.3*).

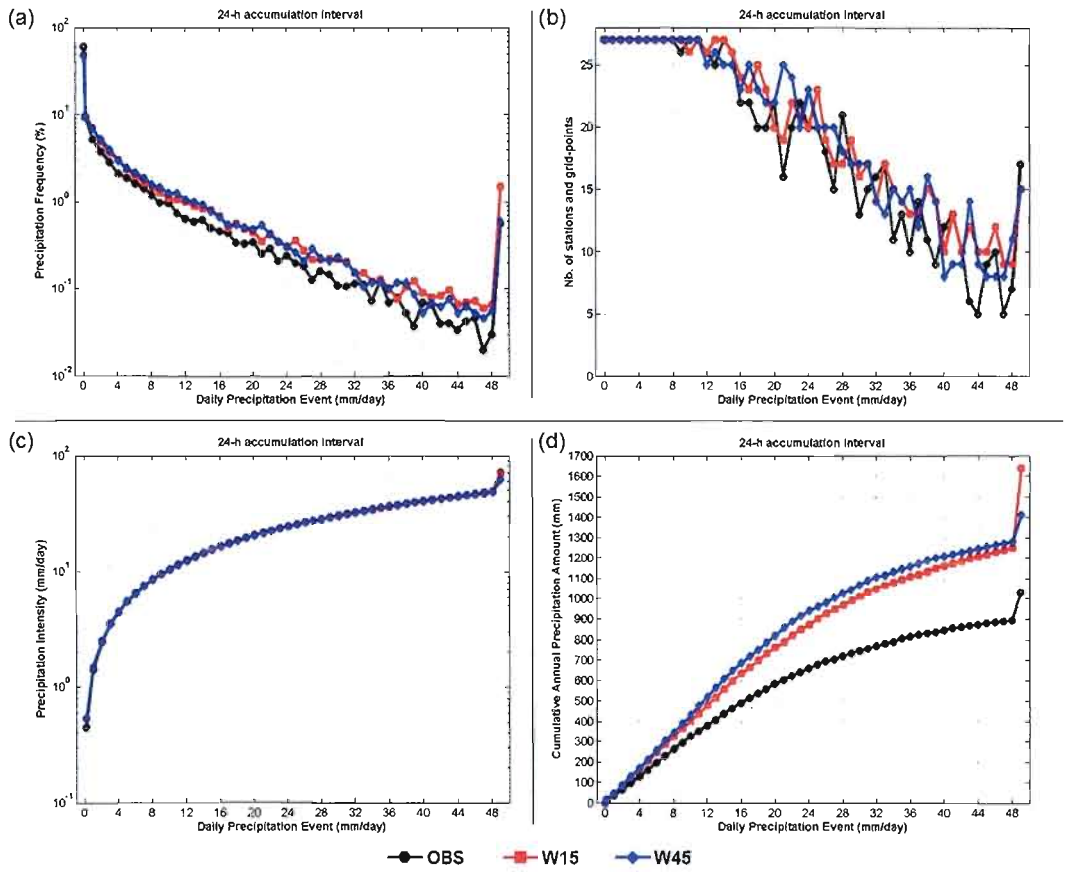

Figure 13 Observed and simulated (W15 and W45) distributions obtained with a 24-h accumulation interval. (a) 4-year mean precipitation frequency (%), (b) 4-year mean number of weather stations (for observations) and grid points (for model), (c) 4-year mean precipitation intensity (mm/h), and (d) 4-year mean cumulative annual precipitation amount (mm). The x-axis represents the Daily Precipitation Event (DPE) in units of mm/day, with the number on the axis being the threshold of a DPE class. The width of each DPE class is 1 mm/day, except for the two first classes (0-0.2 mm/day and 0.2-1 mm/day). On each panel, the curves represent the mean distributions of all the 27 weather stations (for observations) or grid points (for model simulations) used in this study (see section *3.3*).

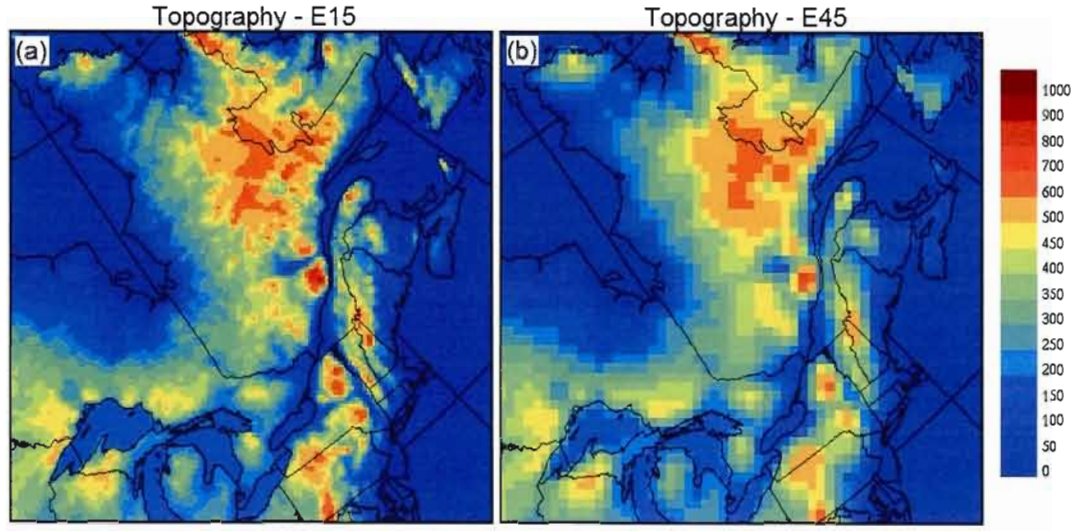

Figure 14 Topography (m) of the simulations E15 (a) and E45 (b).

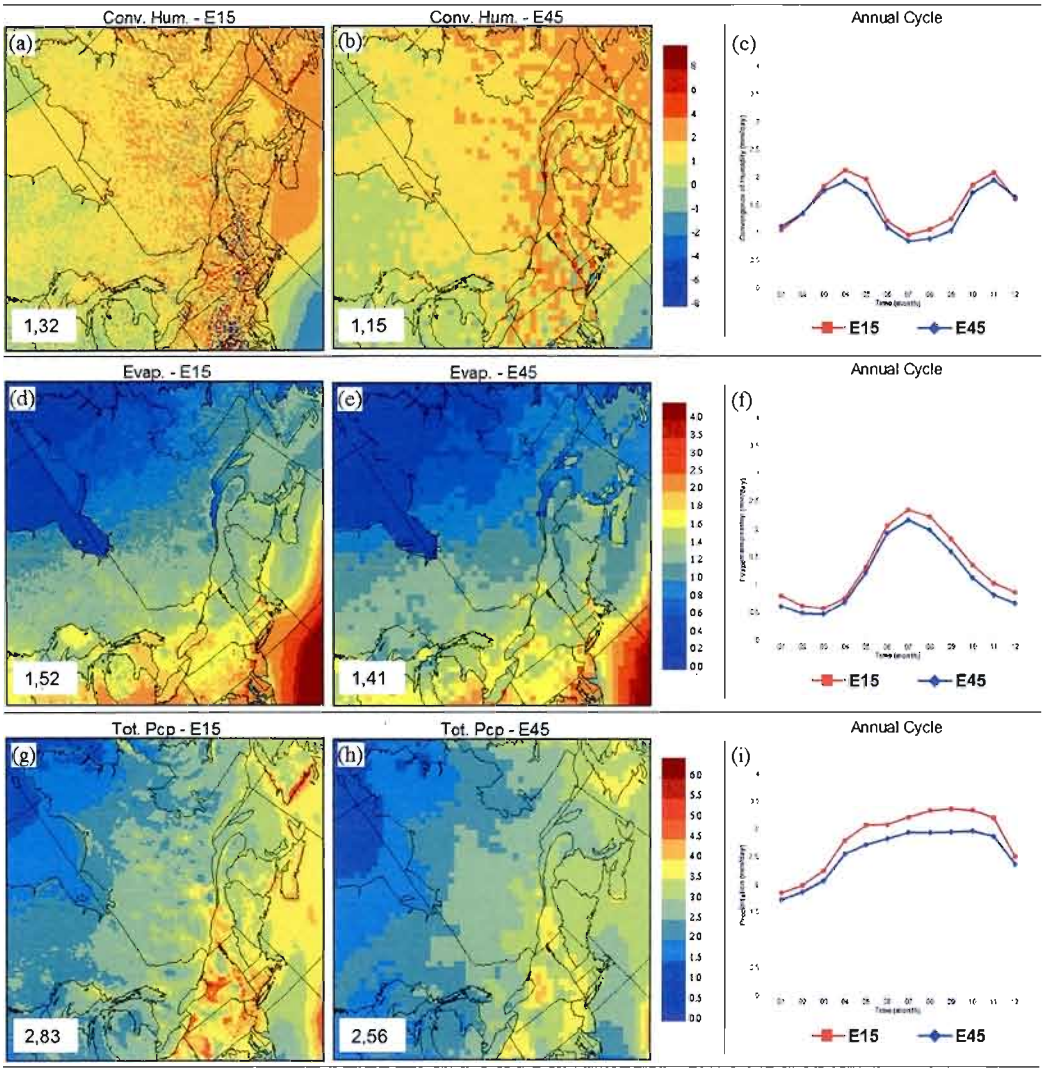

Figure 15 Top: 4-year annual mean convergence of humidity (mm/day) for the simulations E15 (a) and E45 (b). Panel (c) depicts the domain-averaged mean annual cycle of convergence of humidity. Middle: 4-year annual mean evapotranspiration (mm/day) for the simulations E15 (d) and E45 (e). Panel (f) presents the domain-averaged mean annual cycle of evapotranspiration. Bottom: 4-year annual mean total precipitation rate (mm/day) for the simulations E15 (g) and E45 (h). Panel (i) shows the domain-averaged mean annual cycle of total precipitation. On the bottom left corner of panels (a), (b), (d), (e), (g) and (h) is given the domain average of the respective variables.

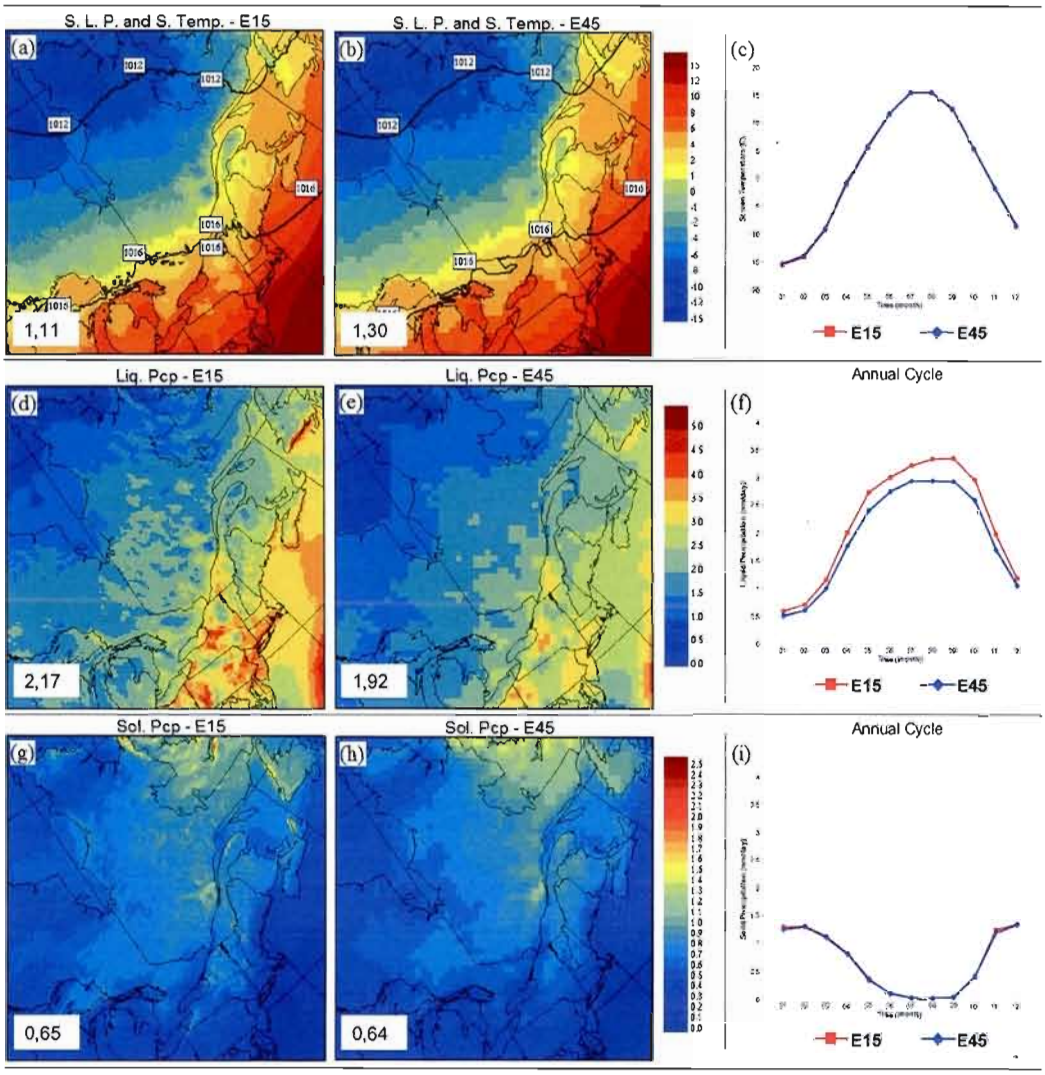

Figure 16 Top: 4-year annual mean sea level pressure (black contours; hPa) and screen temperature (°C) for the simulations E15 (a) and E45 (b). Panel (c) shows the domain-averaged mean annual cycle of screen temperature. Middle: 4-year annual mean liquid precipitation rate (mm/day) for the simulations E15 (d) and E45 (e). Panel (f) presents the domain-averaged mean annual cycle of liquid precipitation. Bottom: 4-year annual mean solid precipitation rate (mm/day) for the simulations E15 (g) and E45 (h). Panel (i) depicts the domain-averaged mean annual cycle of solid precipitation. On the bottom left corner of panels (a), (b), (d), (e), (g) and (h) is given the domain average of the respective variables.

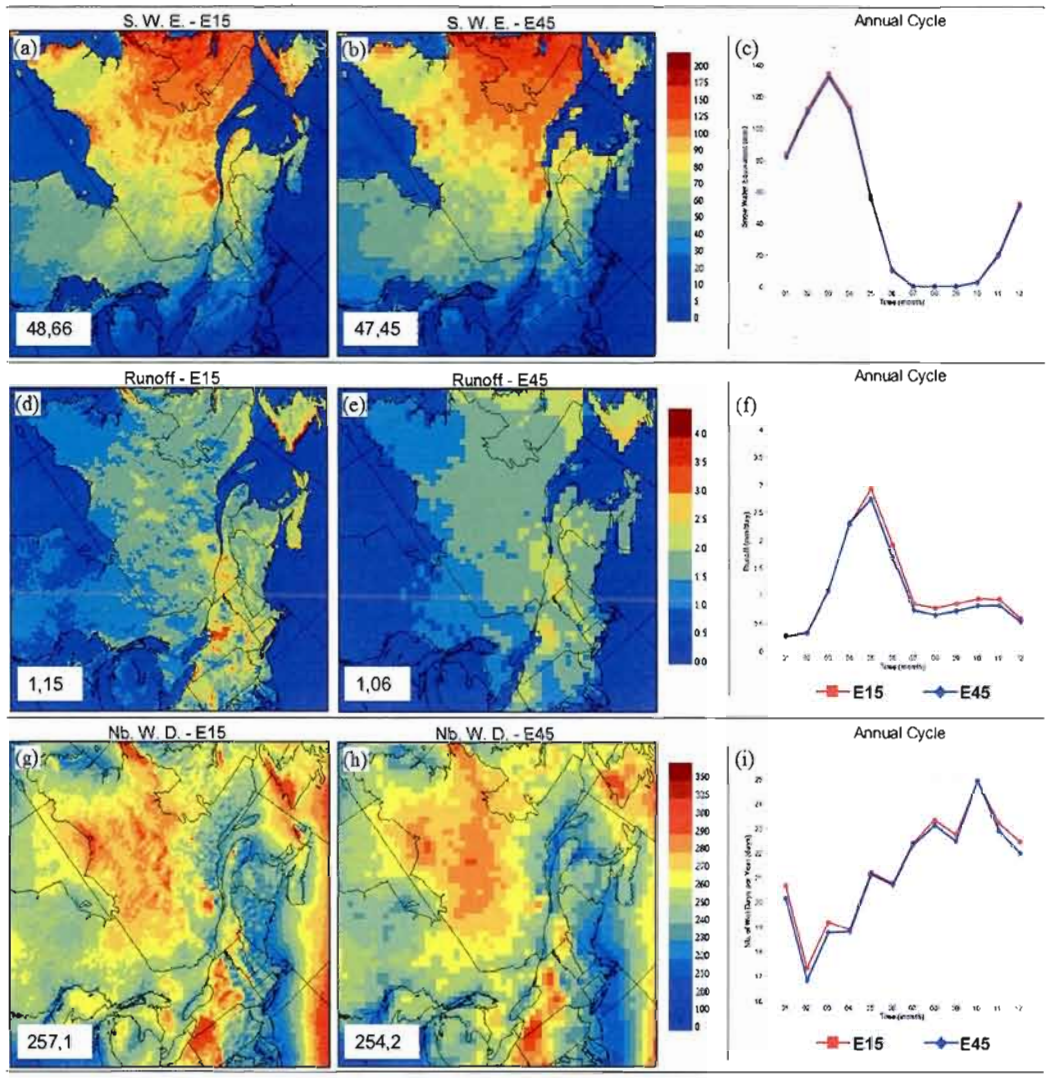

Figure 17 Top: 4-year annual mean snow water equivalent (mm) for the simulations E15 (a) and E45 (b). Panel (c) presents the domain-averaged mean annual cycle of snow water equivalent. Middle: 4-year annual mean runoff (mm/day) for the simulations E15 (d) and E45 (e). Panel (f) shows the domain-averaged mean annual cycle of runoff. Bottom: 4-year mean number of wet days (days/year) for the simulations E15 (g) and E45 (h). Panel (i) presents the domain-averaged mean annual cycle of the number of wet days. On the bottom left corner of panels (a), (b), (d), (e), (g) and (h) is given the domain average of the respective variables.

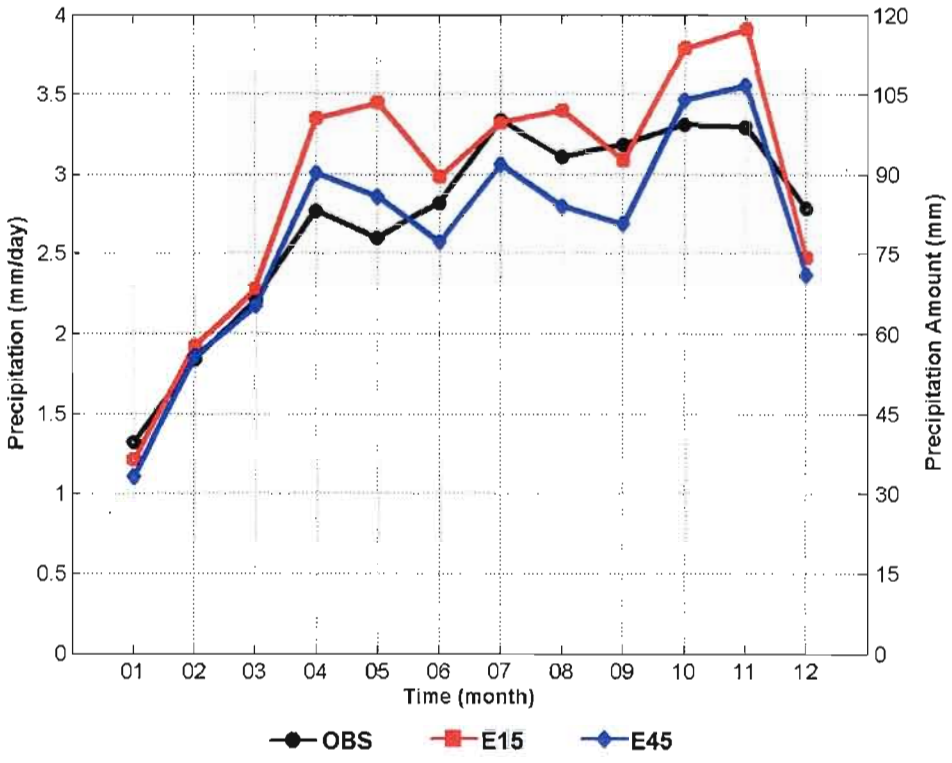

Figure 18 Mean annual cycle of precipitation (mm/day and mm) for model simulations (E15 and E45) and observations. The curves represent the mean annual cycle of all the 45 stations (for observations) or grid points (for model simulations) used in this study (see section *3.3*).

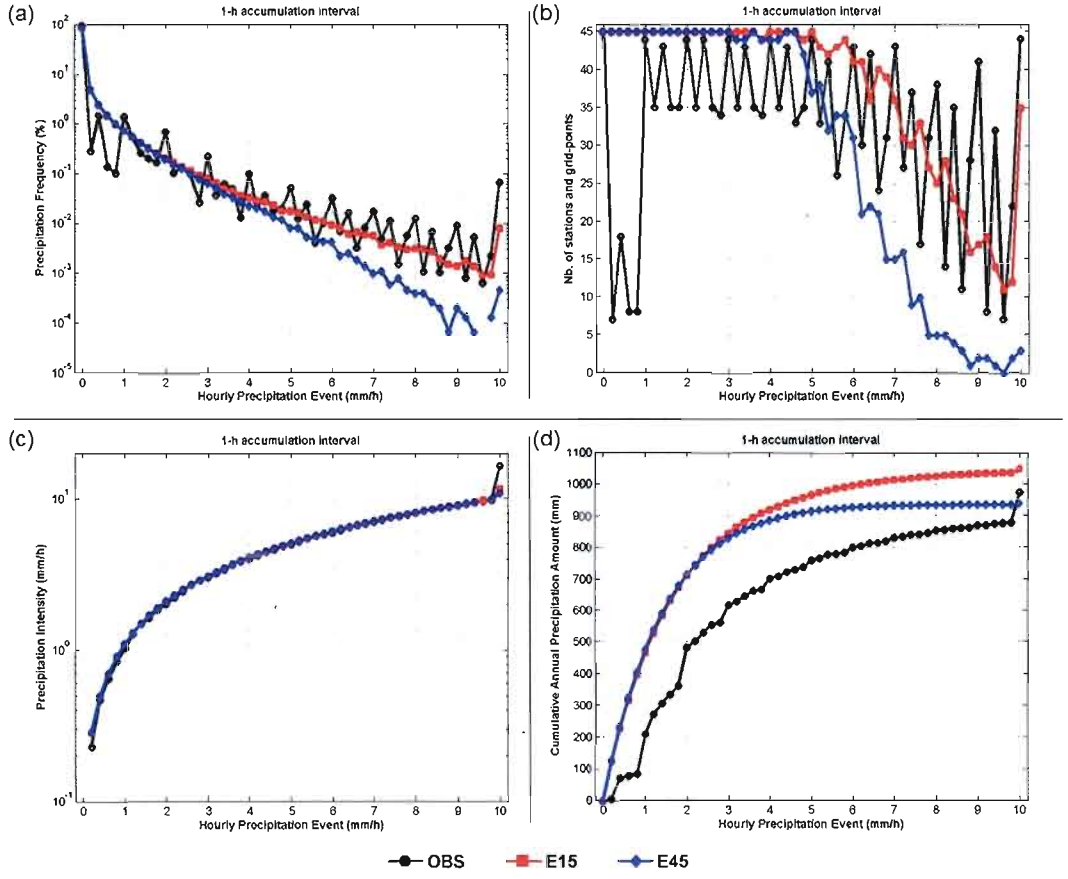

Figure 19 Observed and simulated (E15 and E45) distributions obtained with a 1-h accumulation interval. (a) 4-year mean precipitation frequency (%), (b) 4-year mean number of weather stations (for observations) and grid points (for model), (c) 4-year mean precipitation intensity (mm/h), and (d) 4-year mean cumulative annual precipitation amount (mm). The x-axis represents the Hourly Precipitation Event (HPE) in units of mm/h, with the number on the axis being the threshold of a HPE class. The width of each HPE class is 0.2 mm/h. On each panel, the curves represent the mean distributions of all the 45 weather stations (for observations) or grid points (for model simulations) used in this study (see section *3.3*).

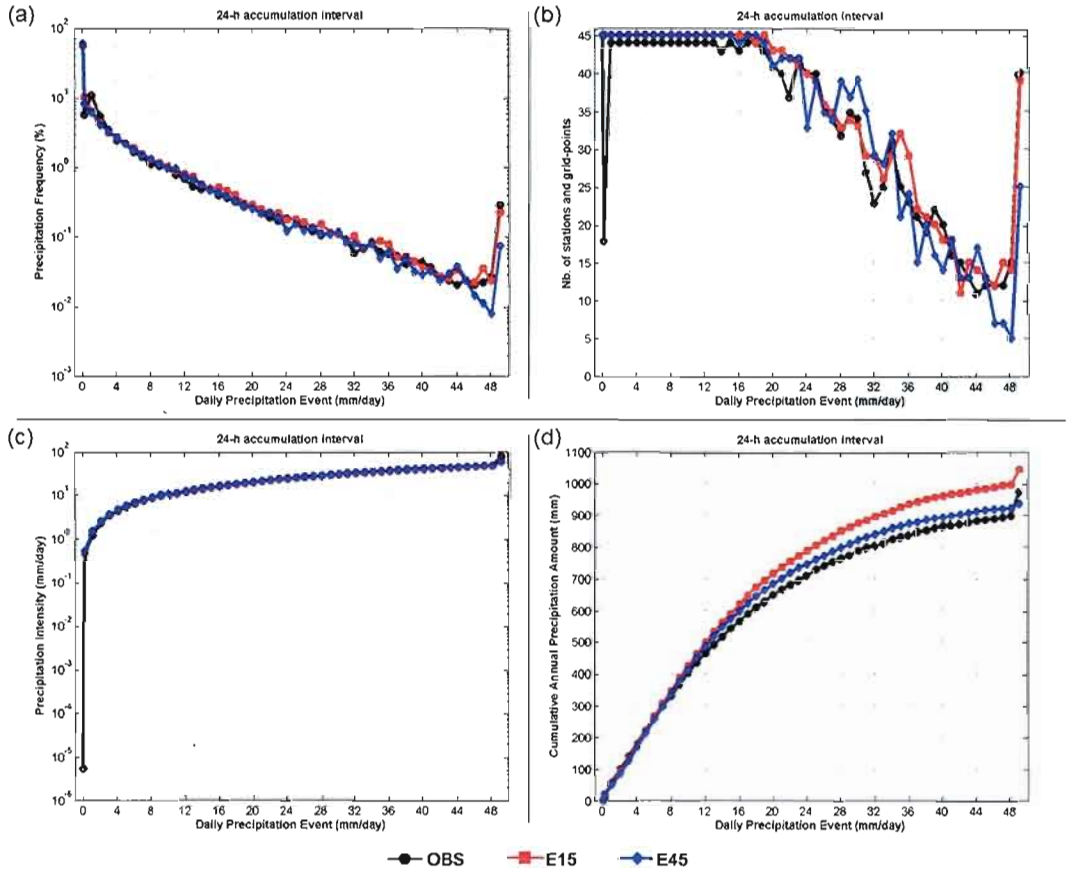

Figure 20 Observed and simulated (E15 and E45) distributions obtained with a 24-h accumulation interval. (a) 4-year mean precipitation frequency (%), (b) 4-year mean number of weather stations (for observations) and grid points (for model), (c) 4-year mean precipitation intensity (mm/h), and (d) 4-year mean cumulative annual precipitation amount (mm). The x-axis represents the Daily Precipitation Event (DPE) in units of mm/day, with the number on the axis being the threshold of a DPE class. The width of each DPE class is 1 mm/day, except for the two first classes (0-0.2 mm/day and 0.2-1 mm/day). On each panel, the curves represent the mean distributions of all the 45 weather stations (for observations) or grid points (for model simulations) used in this study (see section *3.3*).

Figure 21 Geographical positions and abbreviations of the 21 watersheds of interest on the 45-km CRCM grid. Thanks to the Ouranos Consortium for the computer program used to create this figure.

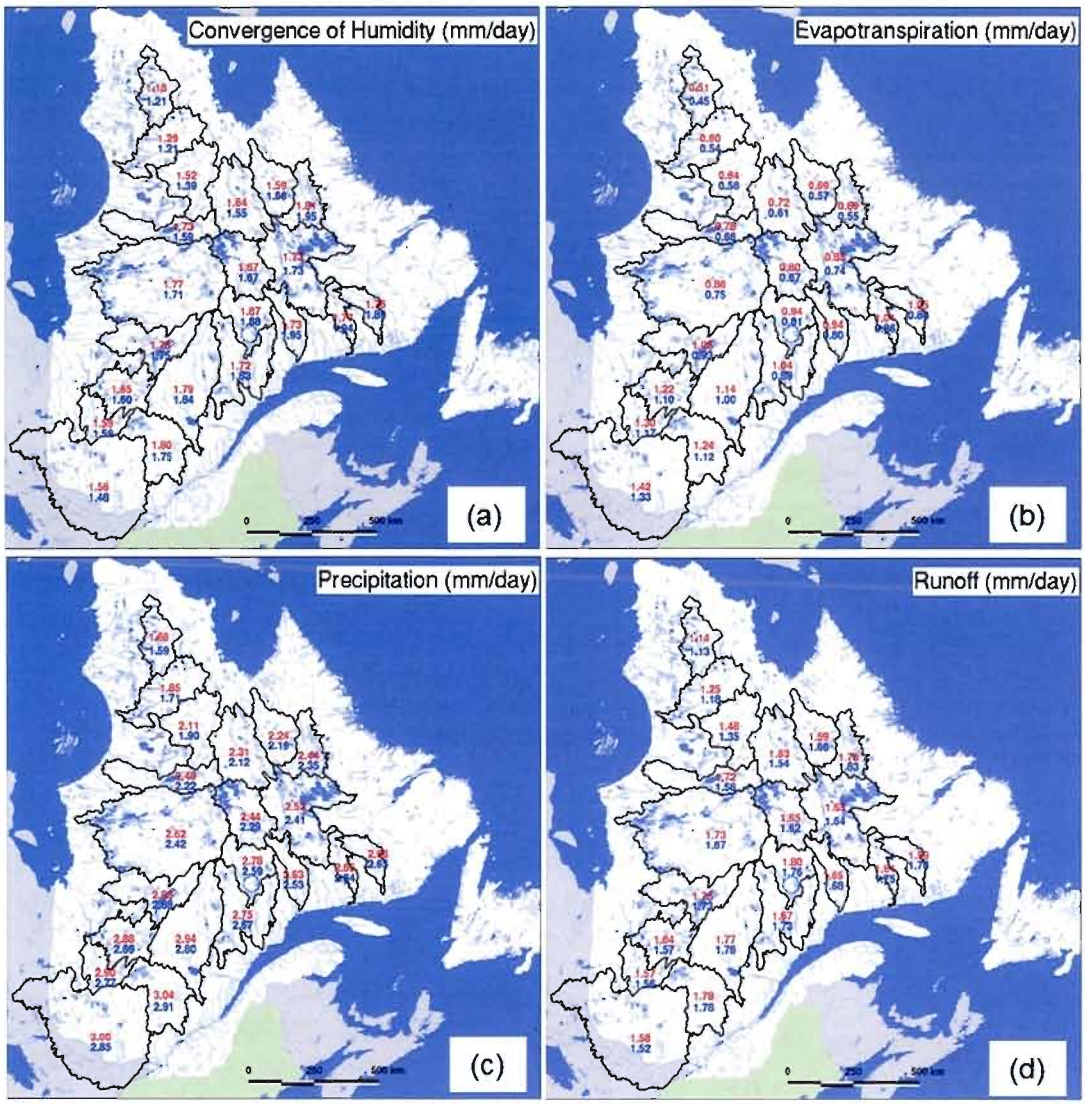

Figure 22 4-year annual mean (a) convergence of humidity (mm/day), (b) evapotranspiration (mm/day), (c) total precipitation (mm/day), (d) runoff (mm/day) over each of the 21 watersheds of interest. Values for the simulation E15 are in red while values for the simulation E45 are in bleu. Thanks to the Ouranos Consortium for the computer program used to create this figure.

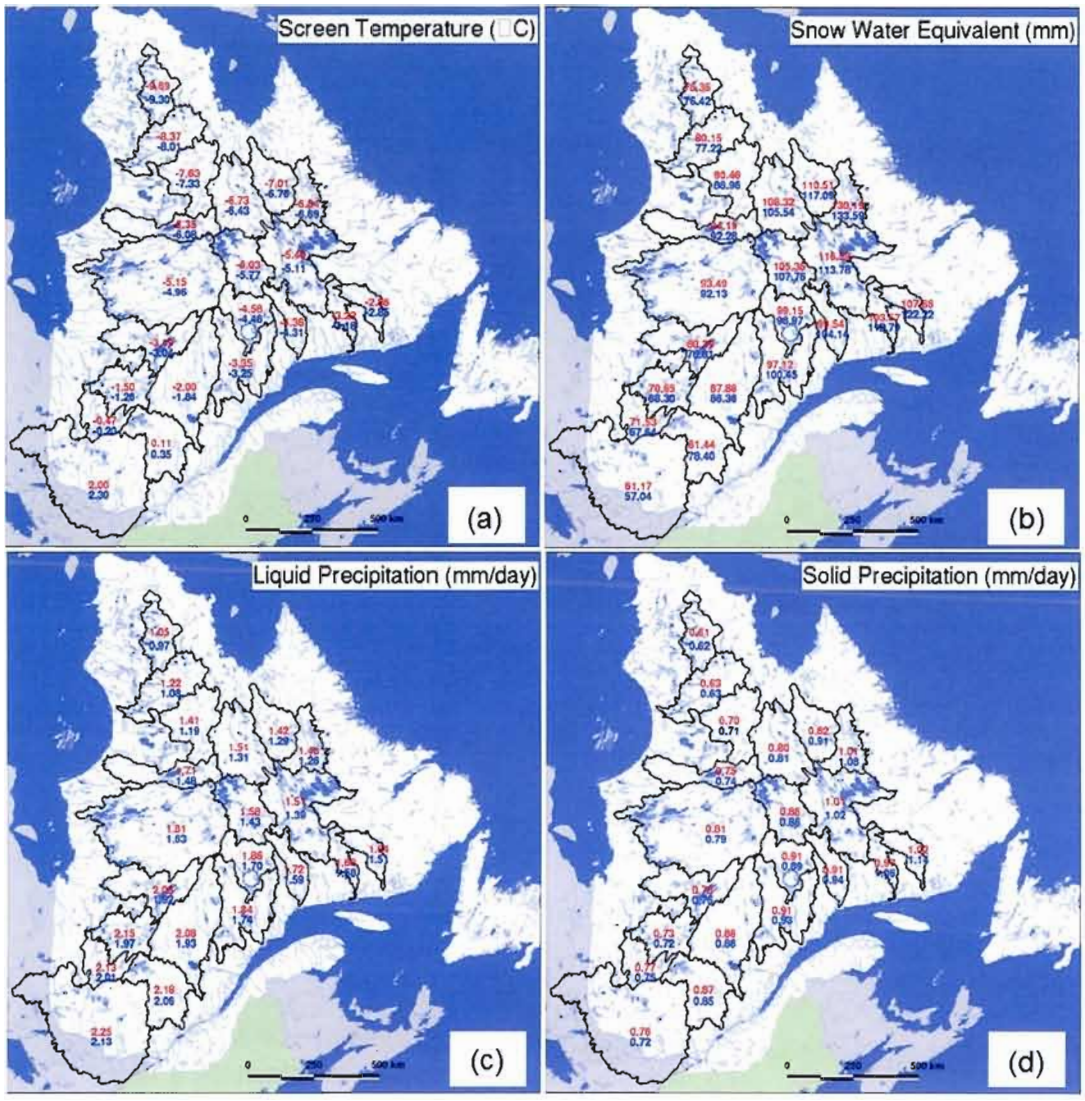

Figure 23 4-year annual mean (a) screen temperature (°C), (b) snow water equivalent (mm), (c) liquid precipitation (mm/day), (d) solid precipitation (mm/day) over each of the 21 watersheds of interest. Values for the simulation E15 are in red while values for the simulation E45 are in bleu. Thanks to the Ouranos Consortium for the computer program used to create this figure.

RÉFÉRENCES

Alexandru A., R. de Elia, R. Laprise, L. Separovic, et S. Biner. 2009. Sensitivity study of Regional Climate Model simulations to large-scale nudging parameters. *Mon. Wea. Rev.*, 137, p. 1666-1686.

Ahrens, C. D. 2003. *Meteorology today - An introduction to weather, climate, and the environment.* 7th ed. Canada: Thomson Learning, 544 p.

Bechtold, P., J. S. Kain, E. Bazile, F. Guichard, P. Mascart, et E. Richard. 2001. A mass flux convection scheme for regional and global models. *Quart. J. Roy. Meteor. Soc.*, 127, p. 869-886.

Caya, D. 1996. «Le modèle régional de climat de l'UQÀM». Thèse de doctorat, Montréal, Université du Québec à Montréal, 134 p.

———, et R. Laprise. 1999. A semi-implicit semi-Lagrangian regional climate model: The Canadian RCM.. *Mon. Wea. Rev.*, 127, p. 341-362.

Chen, M., R. E. Dickinson, X. Zeng, et A. N. Hahmann. 1996. Comparison of precipitation observed over the continental United States to that simulated by a climate model. *J. Climate*, 9, p. 2223-2249.

Christensen, O. B., J. Christensen, B. Machenhauer, et M. Botzet. 1998. Very-high-resolution regional climate simulations over Scandinavia - Present Climate. *J. Climate*, 11, p. 3204-3229.

DAI Catalogue. 2009. *Catalogue available datasets through DAI (Data Access and Integration).* Catalogue version 1.0 (Montréal, avril 2009). Montréal: Environnement Canada, 24 p.

Dai, A., F. Giorgi, et K. E. Trenberth. 1999. Observed and model simulated precipitation diurnal cycles over the contiguous United States. *J. Geophys. Res.*, 104, p. 6377-6402.

Giorgi, F., et M. R. Marinucci. 1996. An investigation of the sensitivity of simulated precipitation to model resolution and its implications for climate studies. *Mon. Wea. Rev.*, 124, p. 148-166.

Groisman, P. Y., R. W. Knight, D. R. Easterling, T. R. Karl, G. C. Hegerl et V. N. Razuvaev. 2005. Trends in intense precipitation in the climate records. *J. Climate*, 18, p. 1326-1350.

Gutowski Jr., W. J., S. G. Decker, R. A. Donavon, Z. Pan, R. W. Arritt, et E. S. Takle. 2003. Temporal-spatial scales of observed and simulated precipitation in Central U.S. climate. *J. Climate*, 16, p. 3841-3847.

Laprise, R., D. Caya, M. Giguère, G. Bergeron, H. Co□té, J.-P. Blanchet, G. J. Boer, et N. McFarlane. 1998. Climate and climate change in western Canada as simulated by the Canadian Regional Climate Model. *Atmos.–Ocean*, 36, p. 119–167.

Mearns, L. O., F. Giorgi, L. McDaniel, et C. Shields. 1995. Analysis of daily variability of precipitation in a nested regional climate model: Comparison with observations and doubled CO_2 results. *Global Planet.* Change, 10, 55-78.

Music, B., et D. Caya 2007. Evaluation of the hydrological cycle over the Mississippi River Bassin as simulated by the Canadian Regional Climate Model (CRCM). *J. Hydrometeor.*, 8, p. 969-987.

———, et D. Caya. 2009. Investigation of the sensitivity of water cycle components simulated by the Canadian Regional Climate Model (CRCM) to the land surface parameterization, the lateral boundary data and the internal variability. *J. Hydrometeor.*, 10, p. 3-21.

———, A. Frigon, M. Slivitzky, A. Musy, D. Caya, et R. Roy. 2009. Runoff modelling within the Canadian Regional Climate Model (CRCM): analysis over the Quebec/Labrador watersheds. *IAHS Publications*, 333, p. 183-194.

Paquin, D., D. Caya et R. Laprise. 2002. Treatment of moist convection in the Canadian Regional Climate Model. *Rapport interne #1 de l'équipe de simulations climatiques à Ouranos, Montréal.* 30 p.

Peixoto, J. P. et A. H. Oort. 1992. *Physics of climate*. American Institute of Physics. 520 p.

Riette, S. et D. Caya. 2002. Sensitivity of short simulations to the various parameters in the new CRCM spectral nudging. *Research activities in Atmospheric and Oceanic Modelling*, edited by H. Ritchie, WMO/TD - No 1105, Report No. 32: 7.39-7.40.

Storch H. V., H. Langenberg, et F. Feser. 1999. A spectral nudging technique for dynamical downscaling purposes. *Mon. Wea. Rev.*, 128, p. 3664-3673.

Sun, Y., S. Solomon, A. Dai, et R. W. Portmann. 2006. How often does it rain? *J. Climate*, 19, p. 916-934.

Trenberth, K. E. 1999. Conceptual framework for changes of extremes of the hydrological cycle with climate change. *Climatic Change*, 42, p. 327-339.

———, A. Dai, R. M. Rasmussen, et D. B. Parsons. 2003. The changing character of precipitation. *Bull. Amer. Metor. Soc.*, 84, p. 1205-1216.

Verseghy, D. L. 1991. CLASS - A Canadian land surface scheme for GCMs. Part I: Soil model. *Int. J. Climatol.*, 11, p. 111–133.

———, N. A. McFarlane, et M. Lazare. 1993. CLASS - A Canadian land surface scheme for GCMs. Part II: Vegetation model and coupled runs. *Int. J. Climatol.*, 13, p. 347–370.

Webster, P. J. 1994. The role of hydrological processes in ocean-atmosphere interactions, *Reviews of Geophysics,* 32, p. 427-476.

Zishka, K. M., et P. J. Smith. 1980. The Climatology of Cyclones and Anticyclones over North America and Surrounding Ocean Environs for January and July, 1950-77. *Mon. Wea. Rev.,* 108, p. 387-401.